

# We are IntechOpen, the world's leading publisher of Open Access books Built by scientists, for scientists

6,900

Open access books available

186,000

International authors and editors

200M

Downloads

Our authors are among the

154

Countries delivered to

TOP 1%

most cited scientists

12.2%

Contributors from top 500 universities



WEB OF SCIENCE™

Selection of our books indexed in the Book Citation Index  
in Web of Science™ Core Collection (BKCI)

Interested in publishing with us?  
Contact [book.department@intechopen.com](mailto:book.department@intechopen.com)

Numbers displayed above are based on latest data collected.  
For more information visit [www.intechopen.com](http://www.intechopen.com)



# Ti-O Film Cathodically-Electrodeposited on the Surface of TiNi SMA and Its Bioactivity and Blood Compatibility

Zhu Weidong

*College of Materials and Metallurgy, Guizhou University,  
China*

## 1. Introduction

### 1.1 Preface

It is easy to prepare  $\text{TiO}_2$  film by electrochemical deposition method technologically. There are some other electrodeposition methods, such as electrophoresis method, anodic-electrodeposition method and cathodic-electrodeposition method.

Tan Xiaochun<sup>[1]</sup> et al. set up a film formation model by electrophoresis method based on experiments and made an exposition of electrophoresis mechanism. The results showed that colloidal concentration and size, DC bias and time are the major factors to form a film. Hayward<sup>[2]</sup> et al. made a investigation of electrophoresis method also.

Nanometer  $\text{TiO}_2$  film prepared by cathodic-electrodeposition is formed in the form of microcrystalline piling up. Kavan<sup>[3]</sup> et al. took  $\text{TiCl}_2$  solution as an electrolyte, to get amorphous Titanium (IV) hydrate film on the anode, and the  $\text{TiO}_2$  film after heat treatment. Cui Xiaoli<sup>[4]</sup> et al. prepared  $\text{TiO}_2$  film on the ITO glass substrate with anodic-electrodeposition method, and investigated the effect of the anodic current and deposition time on nano  $\text{TiO}_2$  structure and adhesive force.

Natarajam<sup>[5]</sup> et al. used Titanium powder as a raw material, which was dissolved with  $\text{H}_2\text{O}_2$  and  $\text{NH}_3$  to get colloid, so that can accomplish the cathodic-electrodeposition on ITO glass in the aqueous solution. Karuppuchamy<sup>[6]</sup> et al. took  $\text{TiOSO}_4$  as a raw material, to prepare  $\text{TiO}_2$  film by cathodic-electrodeposition, the SEM testing results showed that the  $\text{TiO}_2$  film is of porous. When a electrode was photosensitized with dyestuff, the incident light current transform rate of  $\text{TiO}_2$  electrode could reach up to 35%.

Most of cathodic-deposition are accomplished on ITO glass. Chi-Min Lin<sup>[7]</sup> et al. took  $\text{TiCl}_4$  ethylbenzene as an electrolyte, and accomplished the cathodic-electrodeposition on pure Ti. But there are few reports on the study of cathodic-electrodeposition on TiNi SMA. In this experiment, a self-prepared aqueous solution of  $\text{Ti}(\text{SO}_4)_2$  was taken as the electrolyte, the cathodic-electrodeposition of  $\text{TiO}_2$  film on TiNi SMA was achieved. This method is with more convenient in operation, lower cost and easier to accomplish technologically.

## 1.2 Experimental method

### 1.2.1 Experimental materials and media

TiNi shape memory alloy (SMA) (Ti: 49.3 at%, Ni: 50.7%) was used as the experimental material. A sample's size was 20mm×10mm×1mm. The TiNi SMA samples were ground by degrees with abrasive papers (No. W40-W10). After washed ultrasonically with absolute ethyl alcohol and acetone solutions, the samples were put in absolute ethyl alcohol to await for using.

The experimental media were the self-prepared  $\text{Ti}(\text{SO}_4)_2$  solution (PH0.71) of 0.606mg/ml, Hank's solution (making up diluted hydrochloric acid and NaOH solutions into PH7.45) to simulate human body balanced salt solution, and simulated saliva<sup>[8]</sup> (making up lactic acid and ammonia water into PH6.13).

The method of self-preparation of  $\text{Ti}(\text{SO}_4)_2$ :

Weighing out 1.0108g of Titanium dioxide (99.9%) pre-burned at 800°C for 2h, putting it in a platinum crucible with a platinum cover, adding to 3g of potassium pyrosulfate to melt, then putting it in a beaker of 400ml after taken out and cooled; adding sulphuric acid solution of 200ml, leaching the liquid melt at an electric heater, then taking the platinum crucible out and clearing with water, continuing to heat until to the solution clarify entirely, cooling, moving it into a volumetric flask of 1000ml, diluting to the graduation with deionized water, and finally, shaking the flask to be even, in order to get ready to use. And this Ti concentration was 0.06 mg/ml.

Hank's solution composition:

$\text{NaCl}$  8g/l +  $\text{Na}_2\text{HCO}_3$  0.35g/l +  $\text{Na}_2\text{HPO}_4$  0.0475g/l +  $\text{KCl}$  0.4g/l +  $\text{KH}_2\text{PO}_4$  0.06g/l +  $\text{MgCl}_2 \cdot 6\text{H}_2\text{O}$  0.10g/l +  $\text{MgSO}_4 \cdot 7\text{H}_2\text{O}$  0.10g/l +  $\text{CaCl}_2$  0.18g/l + Glucose 1g/l.

Fusayama solution composition:

KCNS 0.52g/l +  $\text{NaHCO}_3$  1.25g/l +  $\text{KCl}$  1.47g/l +  $\text{NaH}_2\text{PO}_4$  0.19g/l + lactic acid 0.75ml.

### 1.2.2 Experimental methods

#### 1.2.2.1 Cathodic-electrodeposition of Ti-O film

A standard trielectrode system was used in the experiment. The device sketch is as shown in figure 1-1. The power supply was DJS-292 type of potentiostat; the reference electrode was saturated calomel electrode (SCE); a TiNi SMA sample was connected with copper wire, its working area was 10mm×10mm, and the non-working area was coated with silica gel; the electrolyte was the self-prepared  $\text{Ti}(\text{SO}_4)_2$  solution.

Before cathodic-depositing the PH value of the  $\text{Ti}(\text{SO}_4)_2$  solution was modified to PH1.2 with 300g/l of KOH solution, adding to 20g/l  $\text{KNO}_3$ . Under this circumstance of that let sample be cathode, at a constant current density of 5mA/cm<sup>2</sup> for 4 min of electrodepositing, a layer of Ti-O film was formed on the surface of TiNi SMA. After finished deposition, the samples were exposed to air for drying naturally, then put them in drying oven for 1h at 120 °C, and then awaited for use.

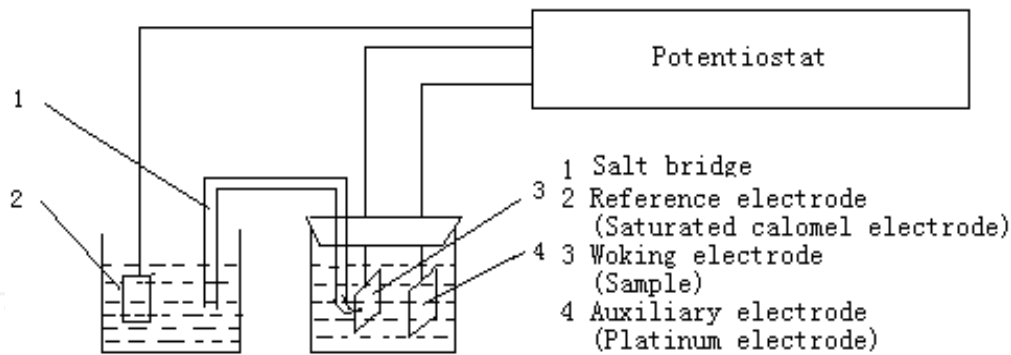


Fig. 1-1. Schematic plan of the trielectrode system

### 1.2.2.2 Composition analysis of Ti-O film

The surface of the sample cathodically-electrodeposited for 4 min at 5mA/cm<sup>2</sup> was observed with XL30 s-FEG type of scanning electronic microscope (SEM). Ti and Ni contents of Ti-O film were analyzed with Finder 1000 type of energy dispersive spectroscopy (EDS). The elemental composition and valent state of Ti-O film were analyzed with MII type of XPS, in order to analyze the film's depositional effect.

The deposited sample was put in a muffle furnace to experience crystallization treatment (annealing) for 1h at 300°C and 450°C respectively, furnace heating and cooling. The phase analysis of Ti-O film was with D/max 2000 type of X-ray diffractometer (XRD).

### 1.2.2.3 Corrosion potential test of the material in simulated physiological environment

Corrosion potential was measured with DJS-292 potentiostat. The connecting diagram is as shown in figure 1-2. The reference cathode was saturated calomel electrode (SCE). The sample was connected with copper wire, its working area was 10mm×10mm, and non-working area coated with silica gel. The samples both before and after cathodic-electrodeposition were dipped into Hank's solution (PH7.45) and Fusayama solution (PH6.13) respectively, then recording the electrode potential and time, potential value recorded once every one minute, until the potential no changing basically. Finally a curve of corrosion potential changed with time could be charted. The experimental parameters were set as in table 1-1.

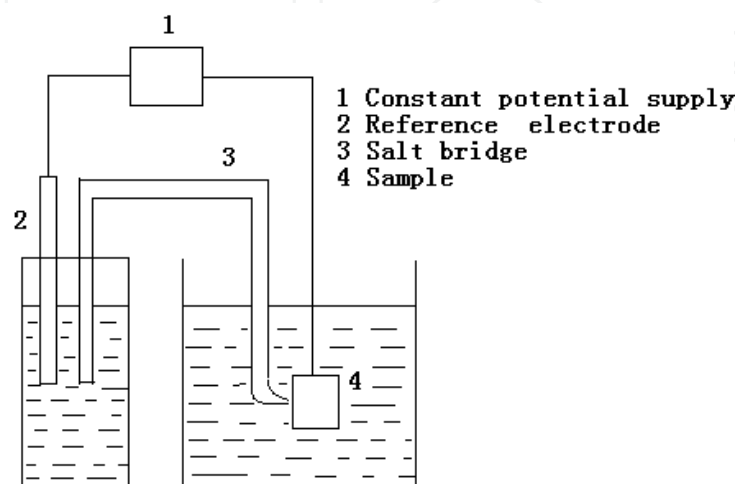


Fig. 1-2. Schematic plan corrosion potential test

Start potential (V/SCE)	Stop potential (V)	Sample interval (mV)	Scanning rate (mV/min)
-0.2	2.0	2	20

Table 1-1. Parameters of dynamic polarization test

#### 1.2.2.4 Potentiodynamic polarization test of the material in simulated physiological environment

The experiment device used a standard trielectrode system. The signal generator used MEC-12 type of multi-function electrochemical analyzer. The reference electrode was SCE. The auxiliary electrode was a Pt one. The sample was connected with a wire, working area 10mm×10mm and non-working area coated with silica gel. The electrolytes were Hank's solution (PH7.45) and Fusayama one (PH6.13). The experiment used the staircase voltage scanning method, to compare and analyze the corrosion resistances of the TiNi SMA before and after cathodic-electrodeposition respectively in simulated physiological environment.

#### 1.2.2.5 Effect of current density on the surface morphology and corrosion resistance of Ti-O film

With an SZX-STAD2 type of OLYMPUS metallurgical microscope, the Ti-O films obtained by cathodic-electrodeposition at different current densities for 4min respectively of TiNi SMA were observed, and the effect of the current densities on surface morphology of Ti-O film were investigated.

The corrosion potential and anodic polarization curve of SMA deposited at 20mA/cm<sup>2</sup> and 5mA/cm<sup>2</sup> in hank's solution and Fuayama solution were respectively tested, in order to investigate the effect of current density on corrosion resistance of Ti-O film.

#### 1.2.2.6 Effect of crystallization treatment on the surface morphology and corrosion resistance of Ti-O film

The samples of TiNi SMA deposited at 20mA/cm<sup>2</sup> for 7min and 5mA/cm<sup>2</sup> for 4min respectively were crystallized at 450°C, with an SZX-STAD2 type of OLYMPUS metallurgical microscope, the Ti-O films before and after depositing respectively were observed, and the effect of crystallization treatment on Ti-O film morphology was investigated.

The TiNi samples deposited at 5mA/cm<sup>2</sup> for 4min before and after crystallizing respectively were taken into Hank's solution (PH7.45) and Fusayama solution (PH6.13) to test their corrosion potential and polarization curve, in order to investigate the effect of crystallization treatment on corrosion resistance of Ti-O film.

#### 1.2.2.7 Effect of deposition time on the surface morphology and corrosion resistance of Ti-O film

Depositing TiNi SMA respectively at a constant current density of 20mA/cm<sup>2</sup> for different times and at another constant current density of 5mA/cm<sup>2</sup> for different times, with an SZX-STAD2 type of OLYMPUS metallurgical microscope, the Ti-O films were observed, to investigate the effect of deposition times at the current densities of 20mA/cm<sup>2</sup> and 5mA/cm<sup>2</sup> respectively on Ti-O film morphology.

### 1.2.2.8 Effect of electrolytes' PH values and NO<sub>3</sub> concentration on cathodic-electrodeposition

With the SZX-STAD2 type of OLYMPUS metallurgical microscope, observation of the Ti-O films obtained by cathodic-electrodeposition for 4min in the electrolytes of PH0.71 and PH1.2 respectively, and the electrolyte without NO<sub>3</sub> added in and electrolyte with 0.02M and 0.2M of NO<sub>3</sub> adding in respectively, were carried out, in order to investigate the effect of PH value and NO<sub>3</sub> concentration on cathodic-electrodeposition.

### 1.2.2.9 Effect of air flow curtain on surface morphology of Ti-O film

Depositing TiNi SMA setting in different bearings, making direction of air flow produced during the TiNi SMA deposition different directions, with the SZX-STAD2 type of OLYMPUS metallurgical microscope, the effect of air flow on Ti-O film morphology was investigated.

## 1.3 Experimental results and discussion

### 1.3.1 Cathodic-electrodeposition of Ti-O film

Under trielectrode system, in mixing well the self-prepared Ti(SO<sub>4</sub>)<sub>2</sub> solution electrolyte, cathodic-electrodeposition was carried out at a constant current density of 5mA/cm<sup>2</sup> for 4min. Because NO<sub>3</sub><sup>-</sup> and H<sub>2</sub>O on the surface of cathode sample obtained electrons to be reduced, making sample surface PH value get high, moreover Ti (IV) could be easily hydrolyzed, so that a layer of amorphousstate Ti-O film was deposited on the surface of TiNi SMA. Its producing process is as following:



The Ti(SO<sub>4</sub>)<sub>2</sub> gel reactively produced was deposited on the surface of the sample.

### 1.3.2 The composition analysis of Ti-O film

Figure 1-3 shows the SEM topography (at different amplifications) of a Ti-O film cathodically-electrodeposited. It can be seen from the figure that under this experimental parameter, the Ti-O film obtained was well-distributedly deposited on TiNi SMA surface. This Ti-O film is closely composed of a lot of tiny particles, the particle's size is in about dozens of nanometers. This close bonding of the particles in nanometer class is conducive to strengthen the TiNi SMA surface properties, and to prevent Ni release from substrate.

Figure 1-4 shows an EDS analysis of the Ti-O film after cathodic-electrodeposition. It can be seen from the figure that this film mainly contains Ti element, as well as a small of amount of Ni element, and the ratio of Ti and Ni reaches 3:1. It illustrates that there is a lot of Ti element in the film. Because EDS might possibly puncture the Ti-O film, thus reflecting the substrate's element, so it could be preliminarily verified that by cathodic-elctrodeposition, a layer of film mainly including Ti element indeed has been deposited on the surface of TiNi SMA.

Figure 1-5 shows an XPS (X-ray photoelectron spectroscopy) analysis result of Ti-O film surface after cathodic-electrodeposition of TiNi SMA. It can be seen from the figure that Ti-O film mainly contains the elements of O and Ti, besides element C (an extraneous pollutant), no Ni element exists.

Figure 1-6 shows a high resolution XPS analysis result of Ti2p in Ti-O film. It can be seen from the figure that there are two peaks, at 458.8eV and 464.6eV respectively, both are Ti quadrivalentcations, corresponding with Ti-O bonding energy at the spin state of  $2p_{3/2}$  and  $2p_{1/2}$ .

Figure 1-7 shows a high resolution XPS analysis result of Ni2p in Ti-O film. It can be seen from the figure that there are no clear peaks emerging, illustrating that no Ni element existing in the Ti-O film.

Figure 1-8 shows a high resolution XPS analysis result of O1s in Ti-O film. It can be seen from the figure that there are two peaks existing, one 530.2eV, this is  $O^{2-}$ ; another one 530.7eV, and this peak is an integrated OH. So, the Ti-O film obtained by cathodic-electrodeposition should exist in the form of  $TiO_2$  or hydrate of  $Ti(OH)_4$ .

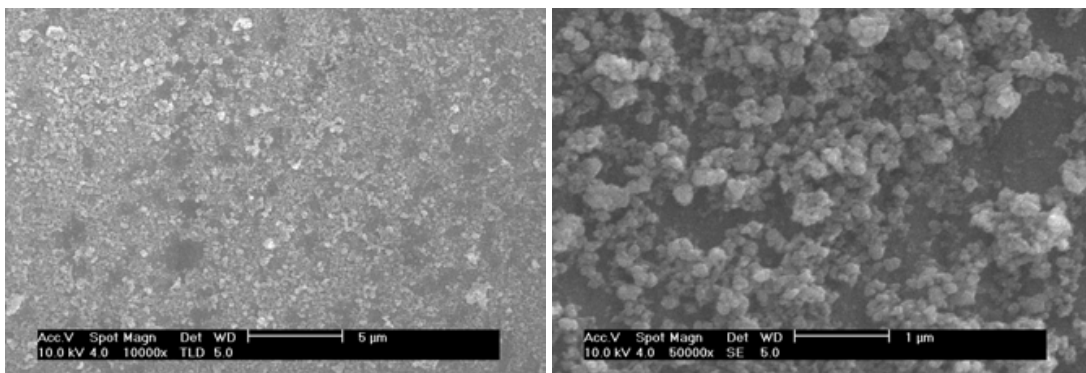


Fig. 1-3. SEM result of Ti-O film

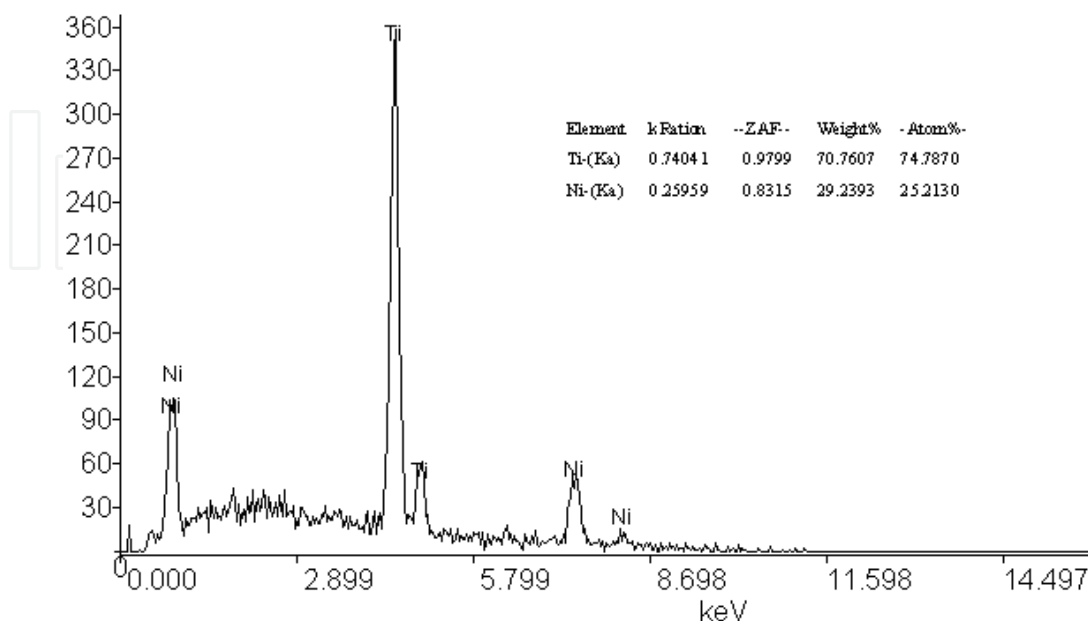


Fig. 1-4. EDS result of Ti and Ni in Ti-O film

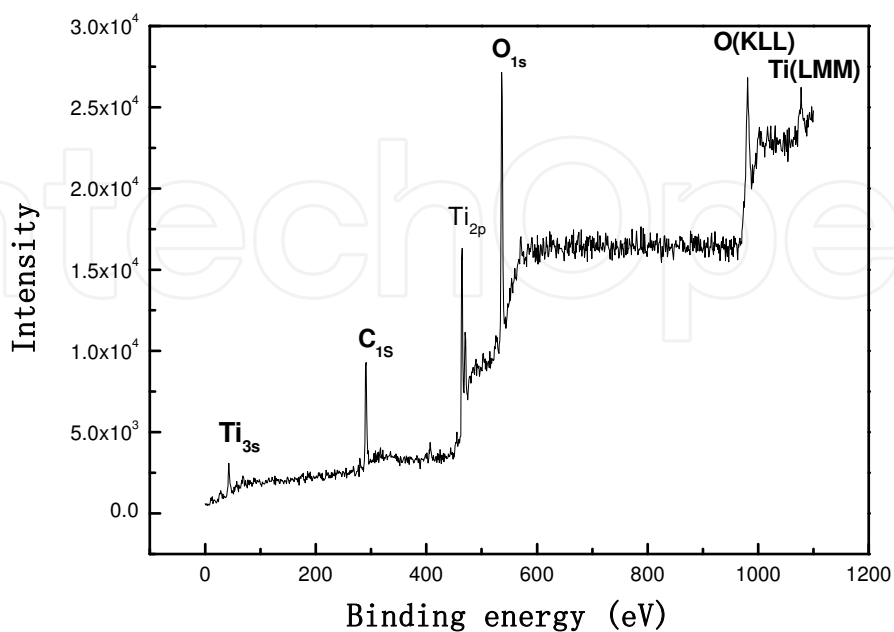


Fig. 1-5. XPS survey spectra of sample cathodically-electrodeposited

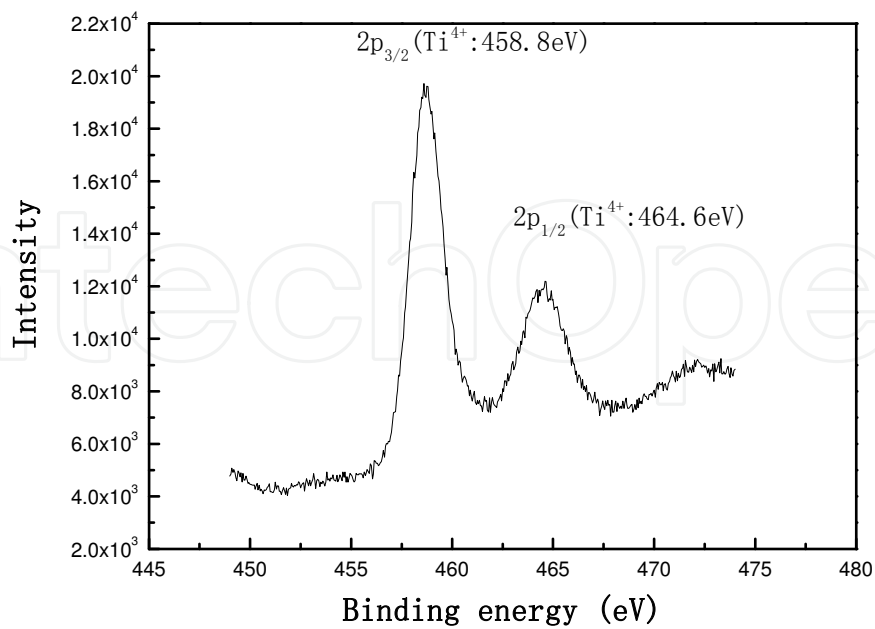


Fig. 1-6. Ti2p XPS energy spectrum of sample cathodically-electrodeposited

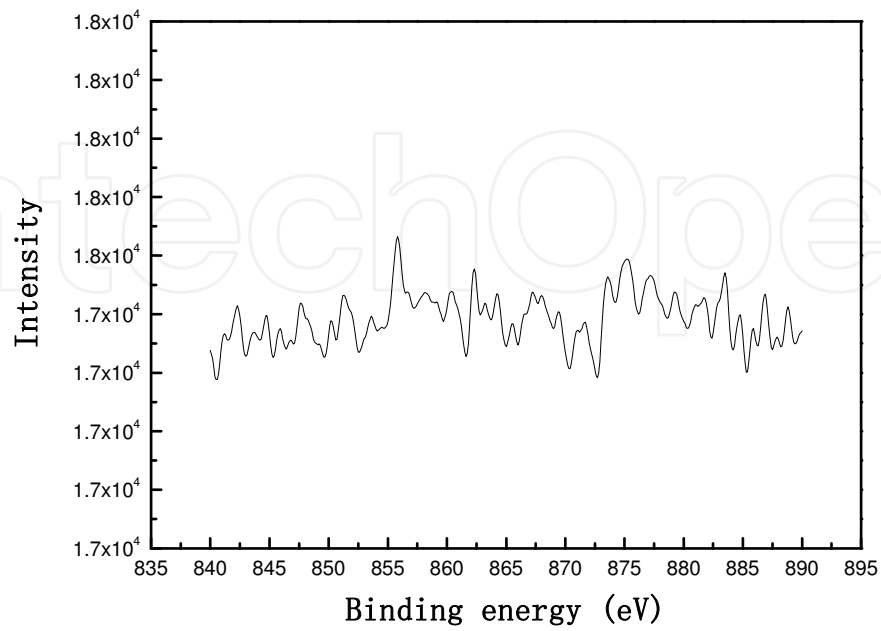


Fig. 1-7. Ni<sub>2p</sub> XPS energy spectrum of sample surface cathodically-electrodeposited

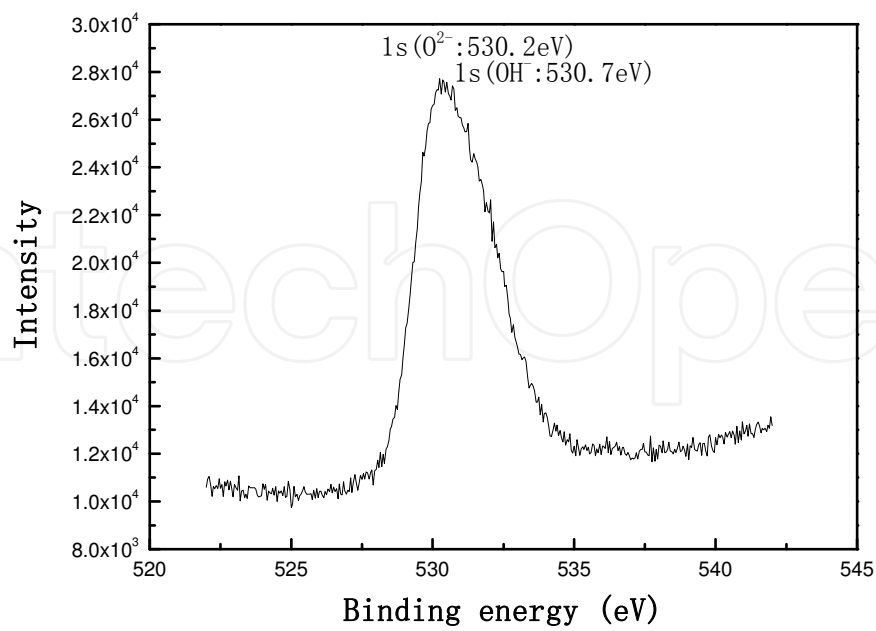


Fig. 1-8. O<sub>1s</sub> XPS energy spectrum of sample cathodically-electrodeposited

Figure 1-9 shows an XRD analysis result of TiNi SMA deposited after heat treatments at different temperatures. It can be seen from the figure that in the Ti-O film crystallized at 300°C, no TiO<sub>2</sub> existing was found besides the main peak reflecting the substrate. But after crystallized at 450°C, there is the peak emerging of anatase TiO<sub>2</sub> in the figure. Because the substrate also has Ti element existing, to investigate if the anatase TiO<sub>2</sub> formed by substrate's thermo oxidation, the same parameters' XRD for the TiNi SMA blank sample before depositing was done. But in the result, no clear TiO<sub>2</sub> peak merged after crystallized at 450°C, this illustrates that the film obtained by cathodic-electrodeposition is truly an amorphous-state Ti-O film, its composition is mainly in the form of hydrate Ti(OH)<sub>4</sub>. The formation of TiO<sub>2</sub> is as the reaction formula:

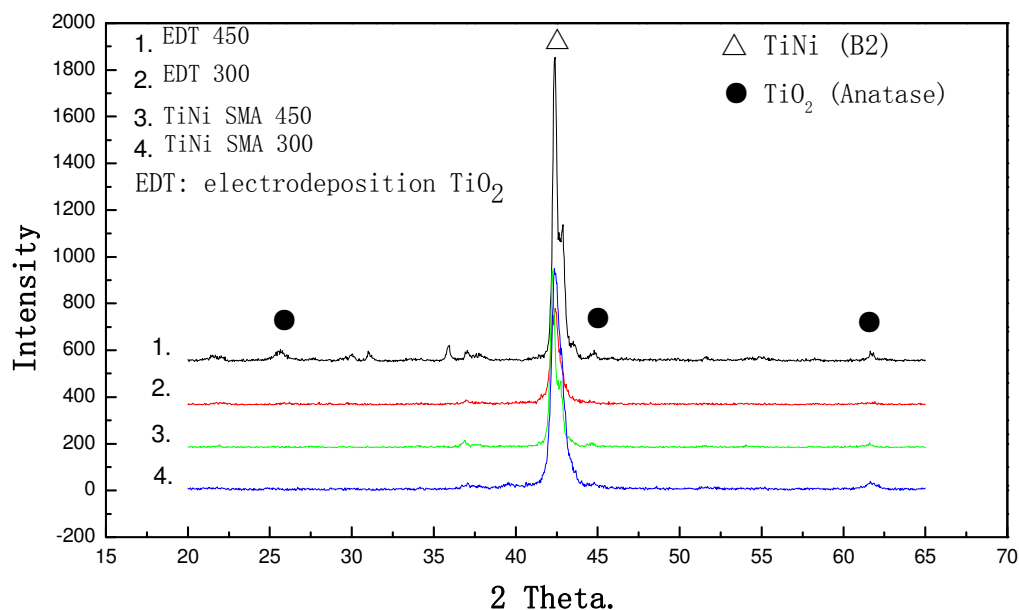


Fig. 1-9. XRD result of heat treated Ti-O film

### 1.3.3 Corrosion potential test of the materials in simulated physical environment

Figure 1-10 shows a relation of corrosion potential-time of the samples before and after depositing in Hank's solution (PH7.45). It can be seen from the figure that the corrosion potential of the deposited sample dipping in solution went down quickly, about 5 minutes after, the corrosion potential did basically not change any more, stabilizing at -0.4V. Furthermore the stable corrosion potential was more positive than the non-depositing sample's, at about -0.2V. This illustrates that the deposited sample has a higher thermodynamic stability than the non-depositing sample's one at PH7.45 in Hank's solution.

Figure 1-11 shows a graph of a relation of corrosion potential-time of the samples before and after depositing in Fusayama solution (PH6.13). It can be seen from the figure that the corrosion potential of the deposited sample dipping in solution went down quickly also, 7 minutes after, basically stabilizing, although somewhat undulating, the potential did not change on the whole, keeping at -0.12V. But the non-depositing sample's potential basically stabilized at -0.15V, which was more negative than the deposited one's. This illustrates that

the deposited sample has a higher thermodynamic stability than the non-depositing sample's one at PH6.13 in Fusayama solution.

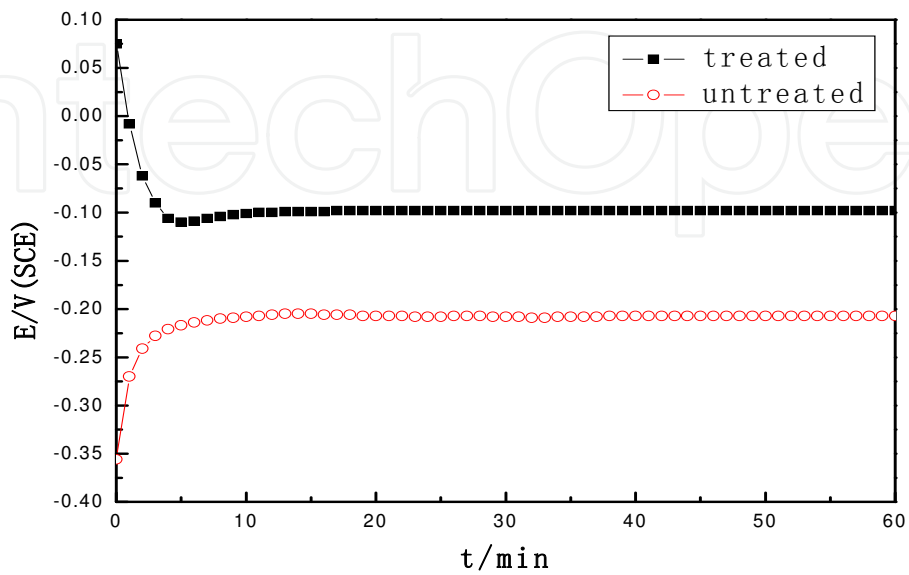


Fig. 1-10. The corrosion potential change plotted as a function of time of samples in Hank's solution (PH7.45)

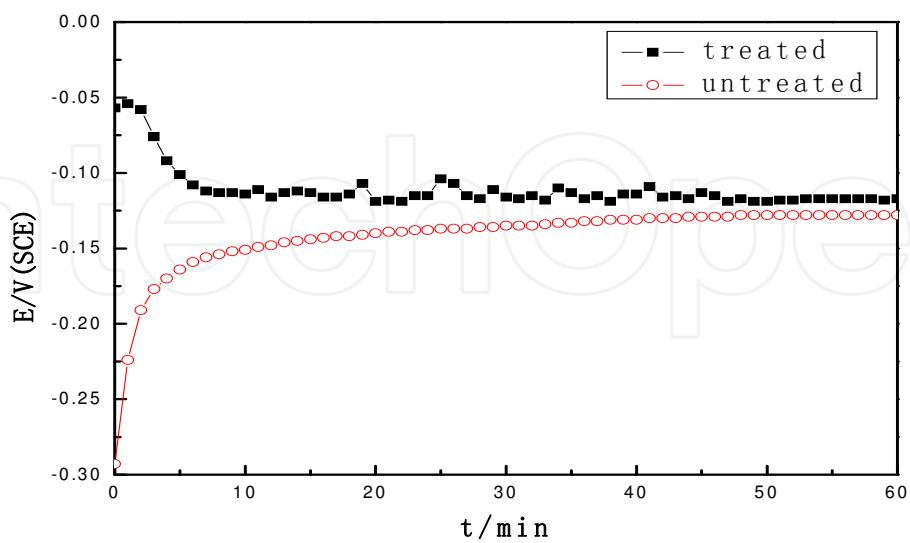


Fig. 1-11. The Corrosion potential change plotted as a function of time of samples in Fusayama solution (PH6.13)

### 1.3.4 Test of potentiodynamic anodic-polarization of the material in simulated physiological environment

Figure 1-12 shows the polarization curves of TiNi SMA before and after cathodic-electrodeposition in Hank's solution (PH7.45). It can be seen from the anodic-polarization curves that the current density of the deposited sample is always lower than that of the one before depositing, even if at passive region, the current density of the deposited sample is similarly lower than that of non-depositing one, and the broken potential of the deposited sample was about 1.2V, and that of non-depositing one about 1.1V, thus the broken potential of the deposited sample was somewhat higher than that of non-depositing one. It can be seen from cathodic-polarization curves that the difference between the two samples' densities is not very great. This illustrates that the cathodically-electrodeposited sample in Hank's solution of PH7.45 has better properties of anodic-polarization and anti-corrosion, and the two properties are approximately close in cathodic-polarization. This is because of the Ti-O film existed on the surface of the deposited sample, with a protective role to substrate, that to a certain extent prevented Ni ions release from substrate, thus having a better corrosion resistance.

Figure 1-13 shows the polarization curves of TiNi SMA before and after cathodic-electrodeposition in Fusayama solution (PH6.13). It can be seen from the polarization curves in the figure that the current density of the deposited sample began to lower than that of non-depositing one from 0.3V, and even at passive region, the current density of the deposited sample was still lower than that of the one before depositing. It can be seen from cathodic-polarization curves that the difference between the two samples' current densities was not great. This also illustrates that because of the Ti-O film existed on the surface of the deposited sample with a protective role to substrate, that to a certain extent prevented Ni ions release from substrate, thus having a better corrosion resistance.

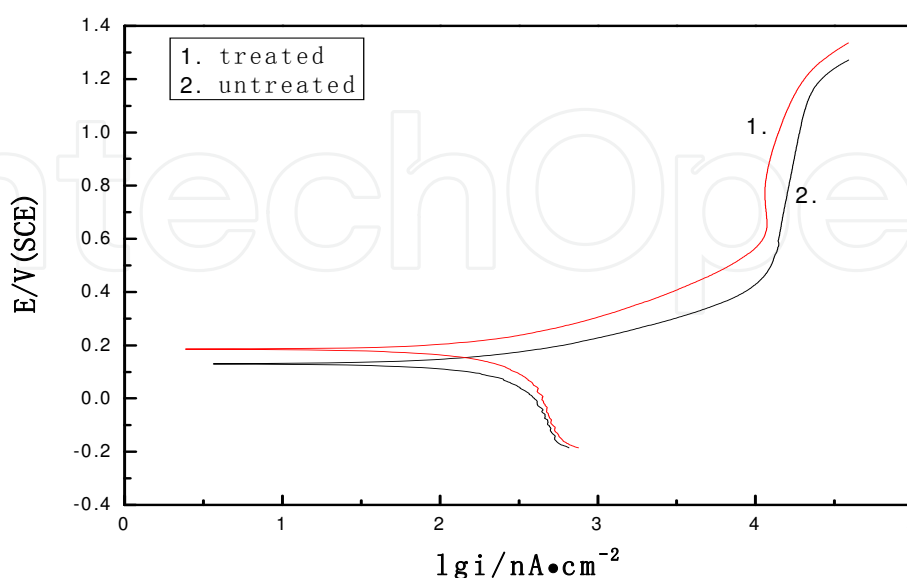


Fig. 1-12. The anodic-polarization curves of samples in Hank's solution (pH7.45)

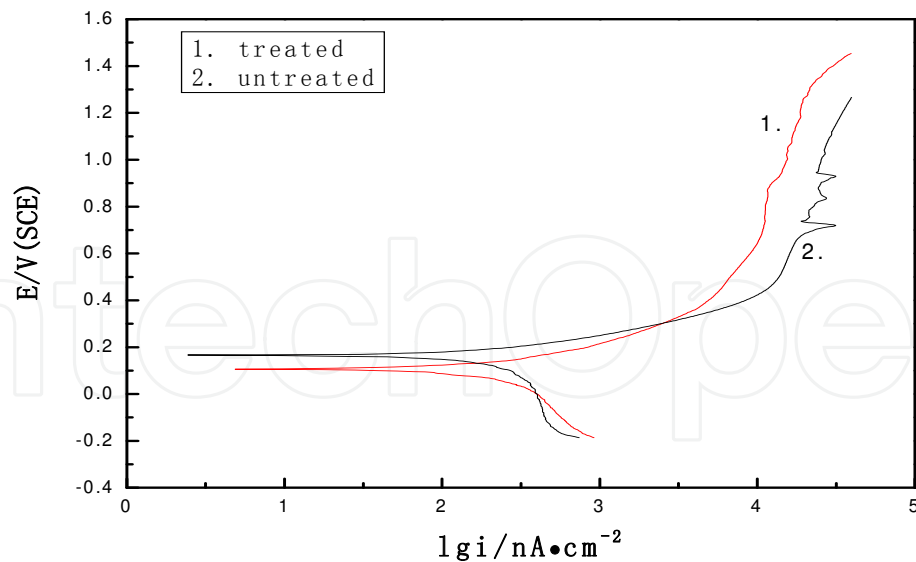


Fig. 1-13. The anodic-polarization curves of samples in Fusayama solution (PH6.13)

### 1.3.5 Effect of current density on surface morphology and corrosion resistance of the film

Figure 1-14 shows the morphologies of under optical microscope at 1000× of amplification of the Ti-O film cathodically-electrodeposited at different current densities. It can be seen from figure a and b that the Ti-O films obtained at 40mA/cm<sup>2</sup> and 30mA/cm<sup>2</sup> were uneven, lumpedly distributed on the surface of TiNi SMA, and with some big cracks; it can be seen from figure c that Ti-O film was fairly even at 20mA/cm<sup>2</sup>, distributed as floc-like on the surface of Ti-O film, but with some considerable cracks; it can be seen from figure d that the Ti-O film obtained at 5mA/cm<sup>2</sup> was fine and close, and with small cracks; from figure e Ti-O film's existence could hardly be seen, only the scratch on the substrate. This illustrates that the Ti-O film obtained at 5mA/cm<sup>2</sup> was the best. Because current density got major, the driving force for Ti(IV) to hydrolyze got major too, Ti-O film quickly formed and grew on the surface of TiNi SMA within a short time. Owing to massedly-produced hydrogen at depositing time, Ti-O film continuously peeled off, thus causing surface very uneven. Besides the film produced at this time was very thick, a stress difference produced due to shrinking in the process of drying, so that many big cracks were brought about. With current density going down, the driving force for Ti(IV) to hydrolyze also getting down, the particles formed getting small, and this made the Ti-O film surface more even, cracks less. But when the current density went down to a certain extent, the driving force for Ti(IV) to hydrolyze would not be enough to form a film on the surface of TiNi SMA.

Figure 1-15 shows the corrosion potential-time curves of the samples athodically-electrodeposited at different current densities in Hank's solution (PH7.45). It can be seen from the figure that the sample deposited at the current density of 20mA/cm<sup>2</sup> had a more positive corrosion potential about -0.2V; but the stable corrosion potential of non-depositing sample was -0.1V. This illustrates that the deposited sample has a better thermodynamic stability at current density of 20mA/cm<sup>2</sup> in the solution. This is because of the Ti-O film deposited at the current density of 20mA/cm<sup>2</sup> was thicker, bonding more closely, that made it have a better thermodynamic stability.

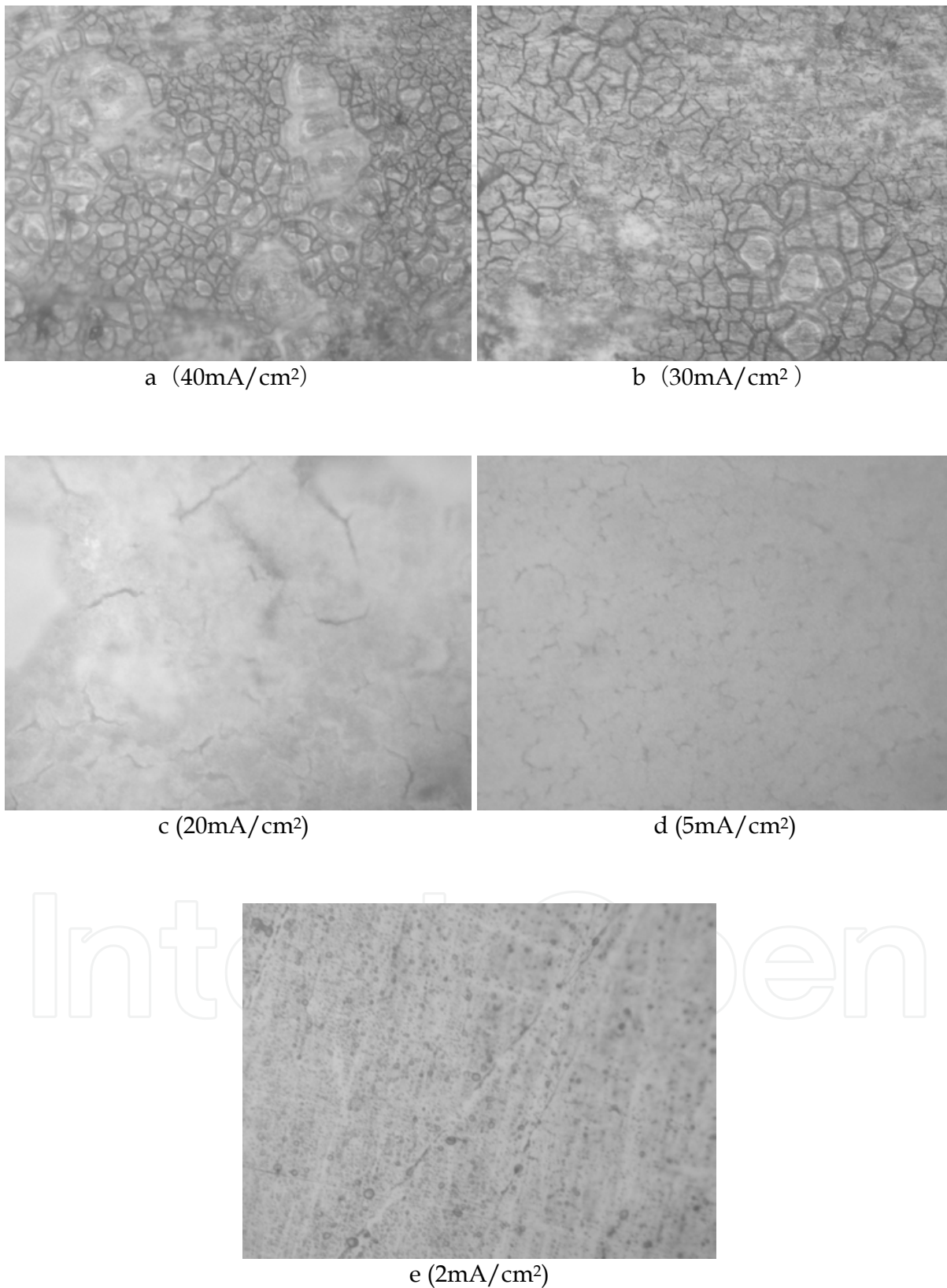


Fig. 1-14. Optical microscope of Ti-O film by different current densities (1000×)

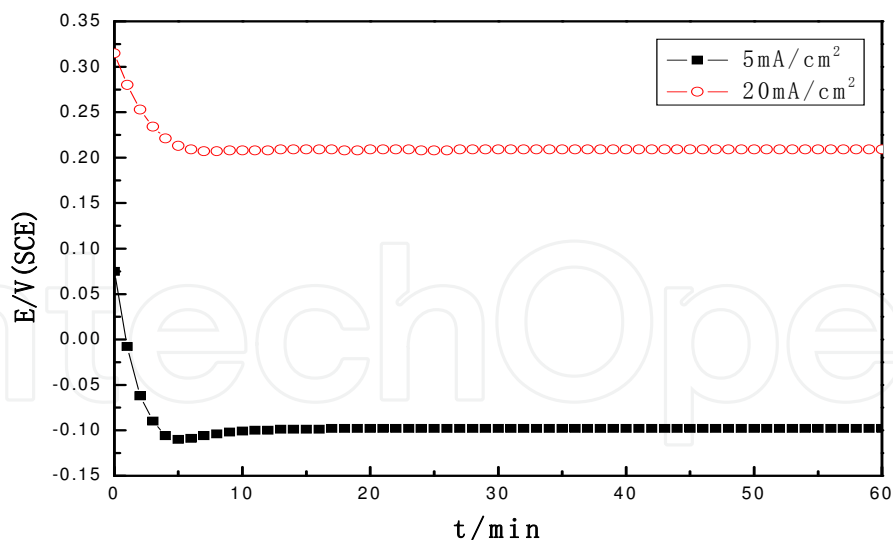


Fig. 1-15. The Corrosion potential change plotted as a function of time of samples with different current densities in Hank's solution (PH7.45)

Figure 1-16 shows the anodic-polarization curves of the samples cathodically-electrodeposited at different current densities in Hank's solution (PH7.45). It can be seen from the anodic-polarization curves in the figure that the deposited samples at current density of  $20\text{mA}/\text{cm}^2$  was much less than the one's at current density of  $5\text{mA}/\text{cm}^2$ , but the passivation region of the deposited sample at current density of  $5\text{mA}/\text{cm}^2$ , was longer than that of the one at high current density. This is because of the Ti-O film of deposited sample at high current density was thicker, which could effectively prevent the ions from transfer, thus making the current density lower. Because the surface of the deposited sample at high current density was very rough, that would bring about the passive film not enough stable after the surface passivated, it is easy to be punctured, so that made the passive region short. But from the figure of view, the slope of the deposited sample at current density of  $20\text{mA}/\text{cm}^2$  is large, it illustrates that the deposited sample has a better cathodic-polarization property.

Figure 1-17 shows the corrosion potential-time curves of the deposited samples at different current densities in Hank's solution (PH7.45) after crystallized at  $450^\circ\text{C}$ . The corrosion potential of the deposited sample at the current density of  $20\text{mA}/\text{cm}^2$  after crystallized was not very stable, undulating much, finally the current potential was about  $-0.205\text{V}$ , which was more negative than that of the one at the current density of  $5\text{mA}/\text{cm}^2$  after crystallized,  $-0.195\text{V}$ . This illustrates that the deposited sample at the current density of  $5\text{mA}/\text{cm}^2$  after crystallized is with a better thermodynamic stability.

Figure 1-18 shows the polarization curves of the deposited samples at different current densities after crystallized at  $450^\circ\text{C}$ . It can be seen from the polarization curves in the figure that the voltage of the deposited sample at current density of  $5\text{mA}/\text{cm}^2$  after crystallized was far lower than that of the one at  $20\text{mA}/\text{cm}^2$ . The breakdown potential of the deposited sample at current density of  $5\text{mA}/\text{cm}^2$  after crystallized was  $1.2\text{V}$ , but the one at  $5\text{mA}/\text{cm}^2$  had no the passivation phenomenon emerging. This illustrates that the deposited sample at current density of  $5\text{mA}/\text{cm}^2$  after crystallized displayed a very good anti-corrosion. Because the granularity of the deposited sample at  $5\text{mA}/\text{cm}^2$  was small, the surface even and very

thin, with less crystal defects, after crystallized and heavy thermalstress, it was easy to corrode, thus presenting a poor corrosion resistance. From the cathodic-polarization curve of view, the deposited sample under current density of  $5\text{mA}/\text{cm}^2$  after crystallized presented similarly a better cathodic-polarization property.

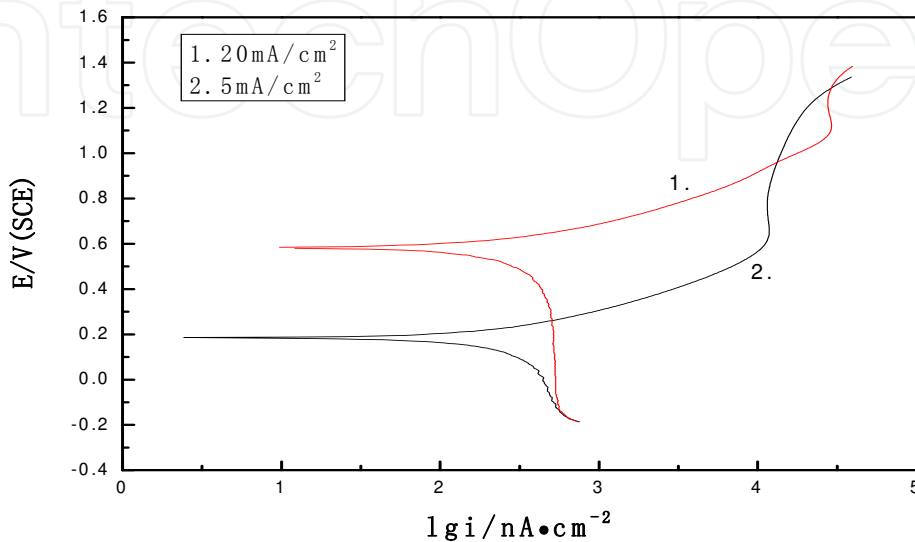


Fig. 1-16. The anodic-polarization curves of samples with different current densities in Hank's solution (PH7.45)

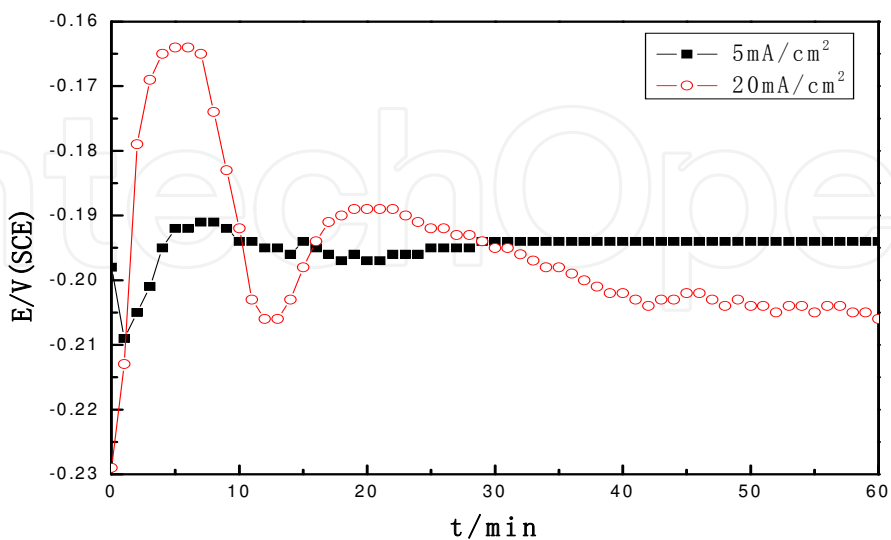


Fig. 1-17. The Corrosion potential change plotted as a function of time of heat treated sample by different current densities in Hank's solution (PH7.45)

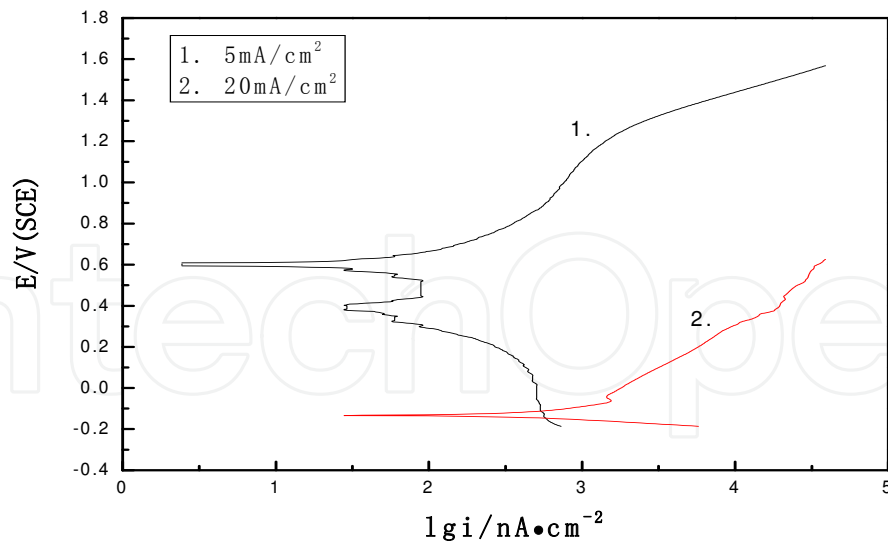


Fig. 1-18. The anodic-polarization curves of heat treated sample by different current densities in Hank's (PH7.45)

Figure 1-19 shows the corrosion potential-time curves of the deposited TiNi SMA samples at different current densities in Fusayama solution of PH6.13. It can be seen that the potentials of both samples moved to more positive direction. The current density of the deposited sample at 20mA/cm<sup>2</sup> had a positive potential, 0.15V, and the stable corrosion potential of the deposited sample at 5mA/cm<sup>2</sup> was -0.12V. This illustrates that the deposited sample at the current density of 20mA/cm<sup>2</sup> in Fusayama solution of PH6.13 has similarly a better thermodynamic stability.

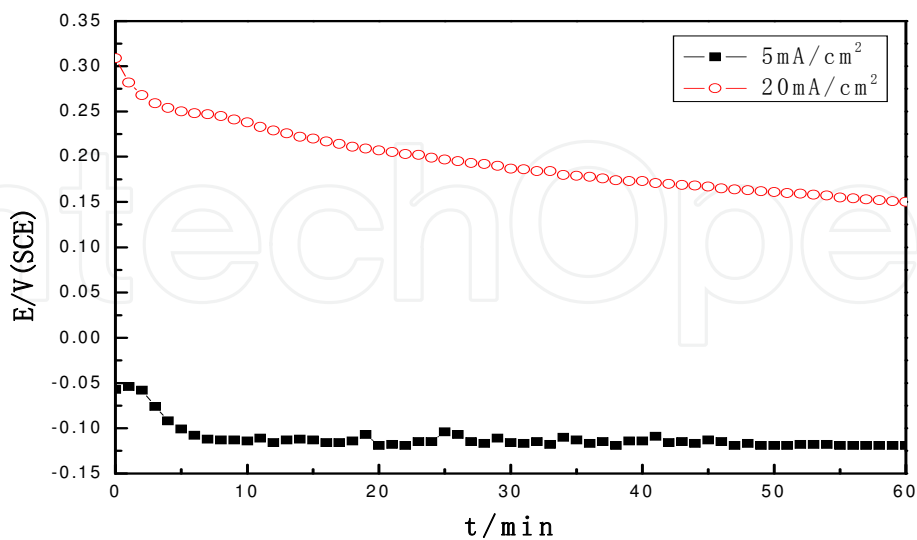


Fig. 1-19. The Corrosion potential change plotted as a function of time of samples with different current densities in Fusayama solution (PH6.13)

Figure 1-20 shows the polarization curves of the deposited TiNi SMA samples at different current densities in Fusayama solution of PH6.13. It can be seen from the polarization curves that in the process of polarization of the deposited sample at the current density of  $5\text{mA}/\text{cm}^2$ , the current density was far higher than that of the one at  $20\text{mA}/\text{cm}^2$ . Although the passivation region of the deposited sample at the current density of  $5\text{mA}/\text{cm}^2$  was longer, its passivation current density was also higher than that of the deposited sample in large range. From the anodic-polarization curves of view as a whole, the deposited sample at the current density of  $20\text{mA}/\text{cm}^2$  had a better corrosion resistance. The reason caused was similar to that the Ti-O film obtained at current density of  $5\text{mA}/\text{cm}^2$  was very thick. From cathodic-polarization curves of view, the deposited sample at the current density of  $20\text{mA}/\text{cm}^2$  similarly presented a better cathodic-polarization property.

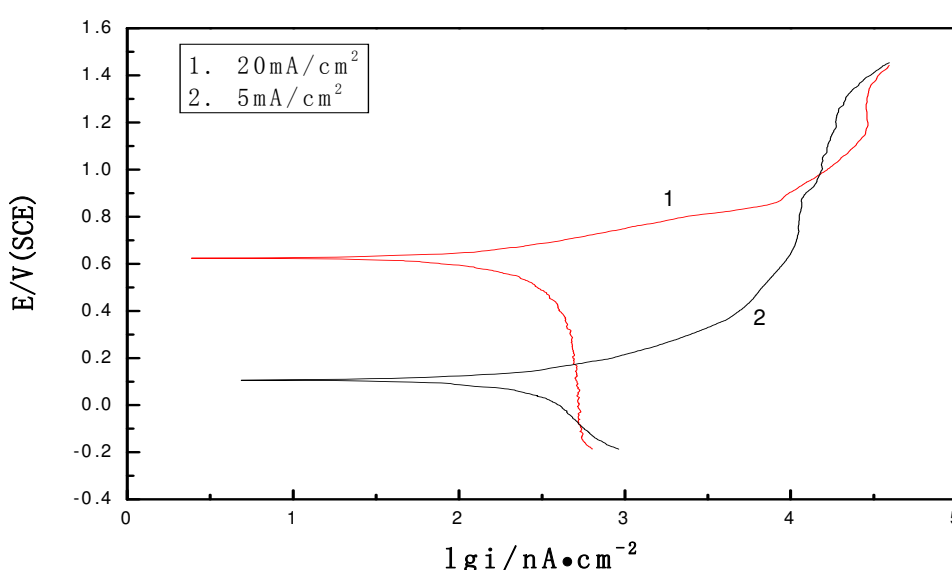


Fig. 1-20. The anodic-polarization curves of samples with different current densities in Fusayama solution (PH6.13)

Figure 1-21 shows the corrosion-potential-time curves of the deposited TiNi SMA samples at different current densities after crystallized at  $450^\circ\text{C}$  in Fusayama of PH6.13. It can be seen from the figure that the corrosion potential of deposited sample at the current density of  $5\text{mA}/\text{cm}^2$  after crystallized went up with time, and the potential did not change basically at about  $-0.19\text{V}$ , but the one at higher current density was in a more negative potential, about  $-0.21\text{V}$ . This illustrates that the sample depositing at the current density of  $5\text{mA}/\text{cm}^2$  after crystallized in Fusayama solution was a continuous formation of a passivation film, its corrosion potential was more positive, and the film presented a better thermodynamic stability.

Figure 1-22 shows the polarization curves of the deposited TiNi SMA samples at different current densities after crystallized at  $450^\circ\text{C}$  in the fusayama solution of PH6.13. It can be seen from the polarization curves that the breakdown potential of deposited sample at the current density of  $5\text{mA}/\text{cm}^2$  after crystallized was  $0.7\text{V}$ , and the current density in the process of polarization was always lower than that of the one at  $20\text{mA}/\text{cm}^2$ , but there was no the passivation phenomenon emerging in depositing the sample. This illustrates that the deposited sample at current density of  $5\text{mA}/\text{cm}^2$  after crystallized had a better property of

anti-corrosion. Similarly, this is because of that the deposited sample at current density of  $5\text{mA}/\text{cm}^2$  was with small granularity, even surface and less crystal defects. From the cathodic-polarization curves of view, the deposited sample at current density of  $5\text{mA}/\text{cm}^2$  after crystallized displayed a better cathodic-polarization property.

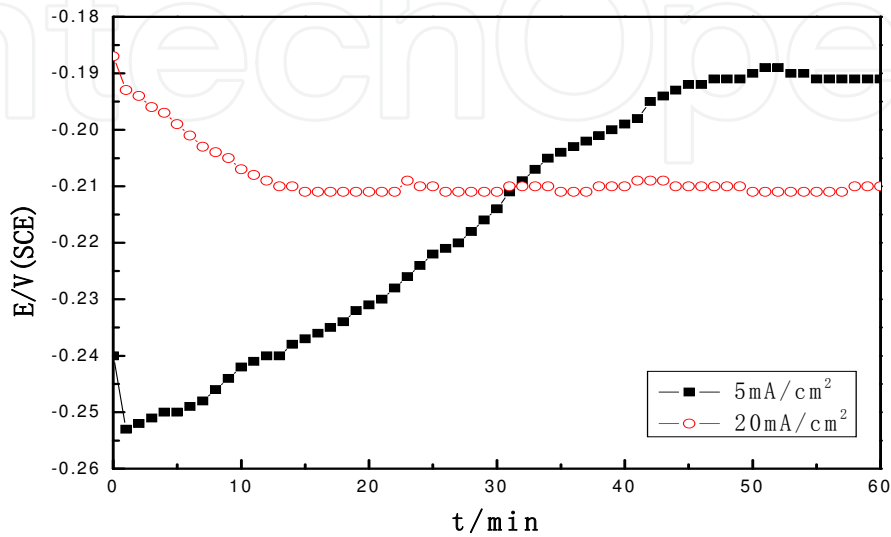


Fig. 1-21. The Corrosion potential change plotted as a function of time of heat treated samples by different current densities in Fusayama solution (PH6.13)

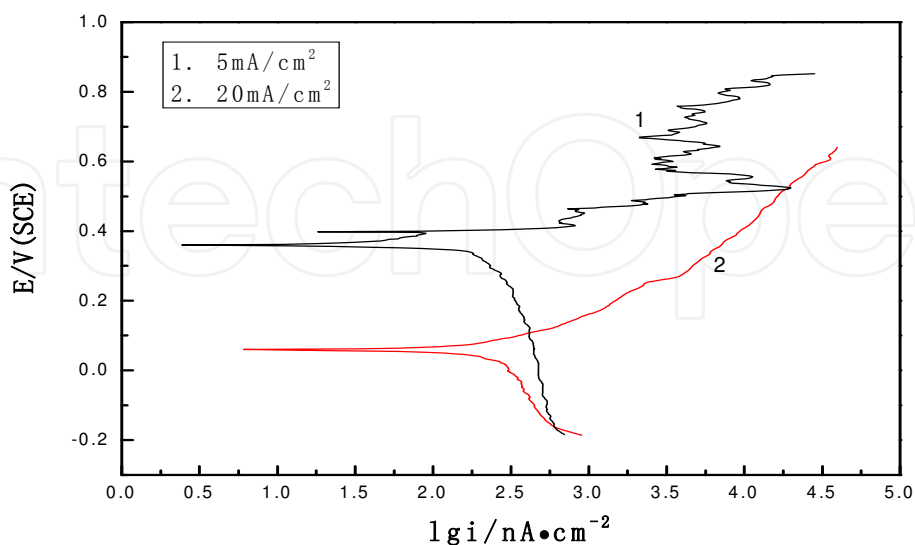


Fig. 1-22. The anodic-polarization curves of heat treated sample by different current densities in Fusayama solution (PH6.13)

### 1.3.6 Effect of crystallization treatment on surface morphology and corrosion resistance

Figure 1-23 shows the optical microscope morphologies of the deposited samples at the current density of  $20\text{mA}/\text{cm}^2$  for 7min before and after crystallization. It can be seen from figure 1-21a and figure 1-21b that before crystallization the surface Ti-O film, presenting bigger lump in shape, covered on the surface of TiNi SMA; it can be seen from figure 1-21c and figure 1-21d that the crystallized Ti-O film in smaller lump in shape distributed on the substrate surface. This is because of that the crystallization treatment made the hydrate (mainly  $\text{Ti}(\text{OH})_4$ ) of amorphous Ti dehydrate water molecules and the crystal lattice recombine to form the anatase type of  $\text{TiO}_2$ . Due to that the current density in cathodic-electrodeposition was higher, the Ti-O film obtained was thicker too, so, in the process of crystallization, there might be uneven dehydration and stress distribution existing, thus bringing about serious crystal defects to affect the properties of Ti-O film to a large extent.

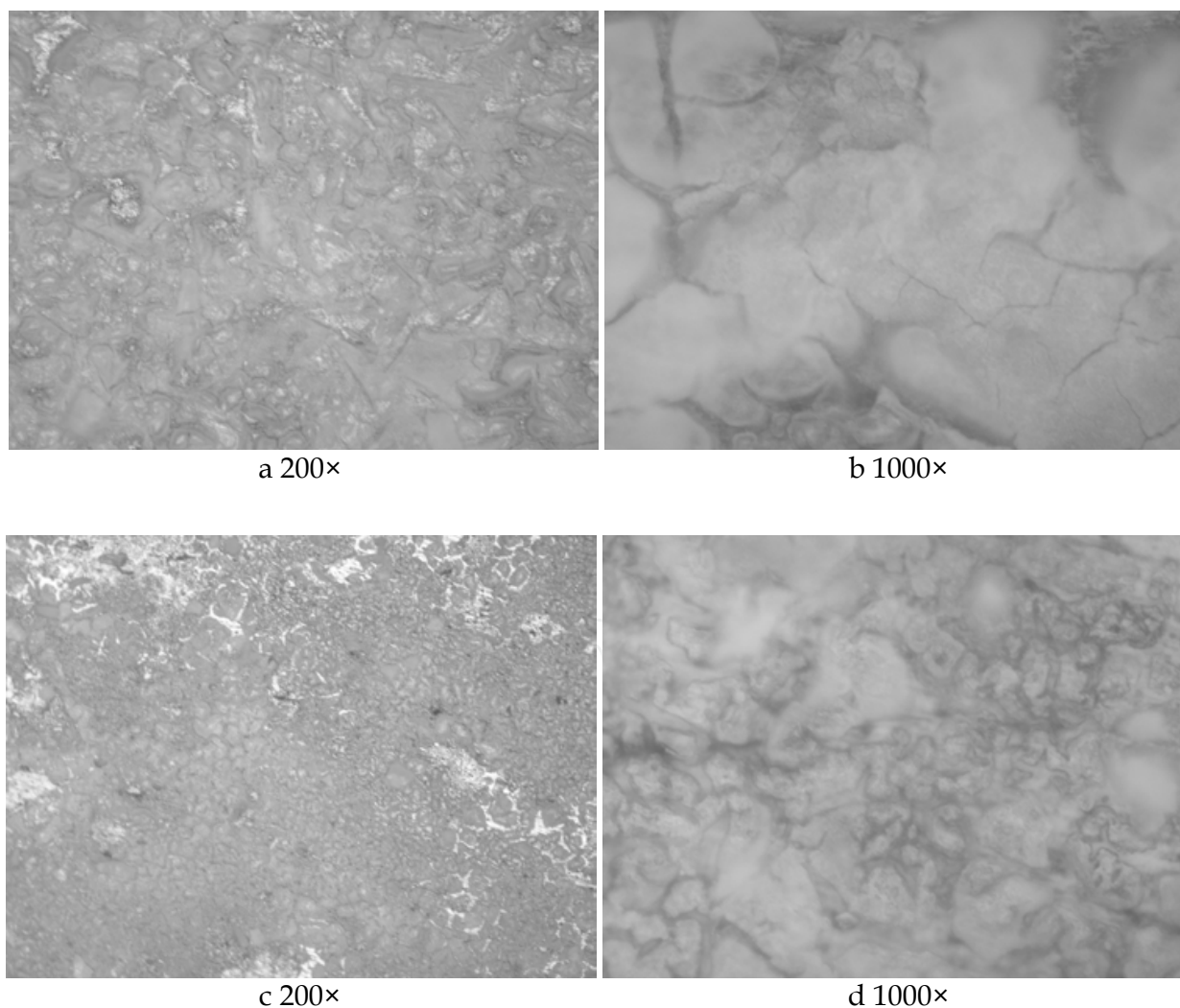


Fig. 1-23. Optical microscope result by current  $20\text{mA}/\text{cm}^2$  for 7 min (a, b untreated; c, d heat treated)

Figure 1-24 shows the optical microscope morphologies of the deposited samples at current density of  $5\text{mA}/\text{cm}^2$  for 4min before and after crystallization. It can be seen from figure 1-22a and 1-22b that Ti-O film was even and smooth, and from 1-22c and 1-22d that the film distributed in type of tiny particles. Similarly, this is because of that the crystallization treatment made the hydrate (mainly  $\text{Ti}(\text{OH})_4$ ) of amorphous Ti dehydrate water molecules and the crystal lattice recombine to form the anatase type of  $\text{TiO}_2$ . Because the film was thinner, the crystal defects caused in the process of crystallization was less, so that the effect on the film's properties would not be serious.

Figure 1-25 shows the corrosionpotential-time curves of the deposited samples at current density of  $5\text{mA}/\text{cm}^2$  before and after crystallization in Hank's solution of PH7.45. it can be seen from the figure that the corrosion-potential of the sample before crystallization basically reached a stability at 5min, about  $-0.1\text{V}$ ; and that of the crystallized one was about  $-0.19\text{V}$ , presenting a more negative potential. This illustrates that in the Hank's solution of PH7.45, the deposited TiNi SMA sample at current density of  $5\text{mA}/\text{cm}^2$  before crystallization displayed a better thermodynamic stability.

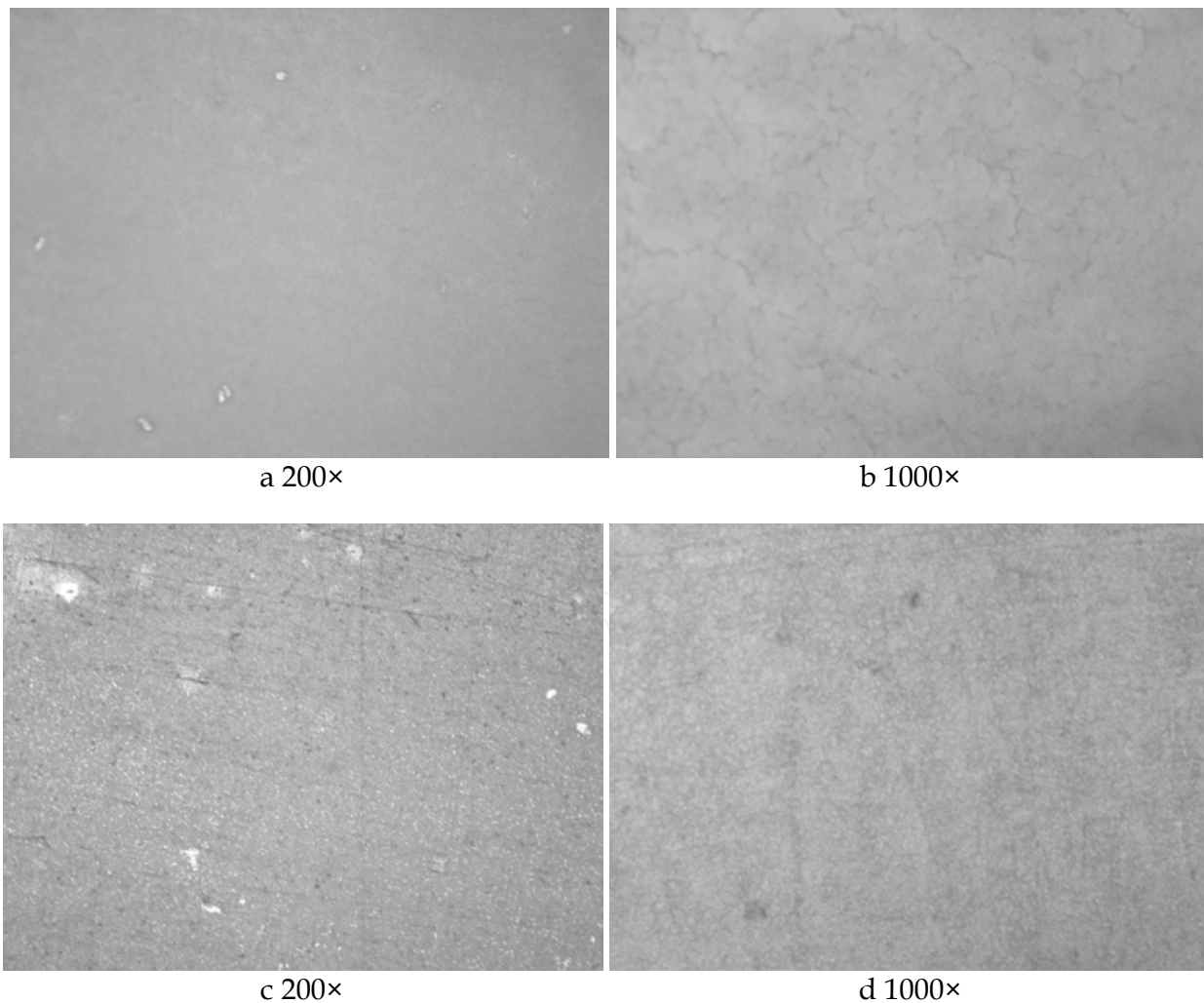


Fig. 1-24. Optical microscope result by current  $5\text{mA}/\text{cm}^2$  for 4 min (a, b unannealed; c, d annealed)

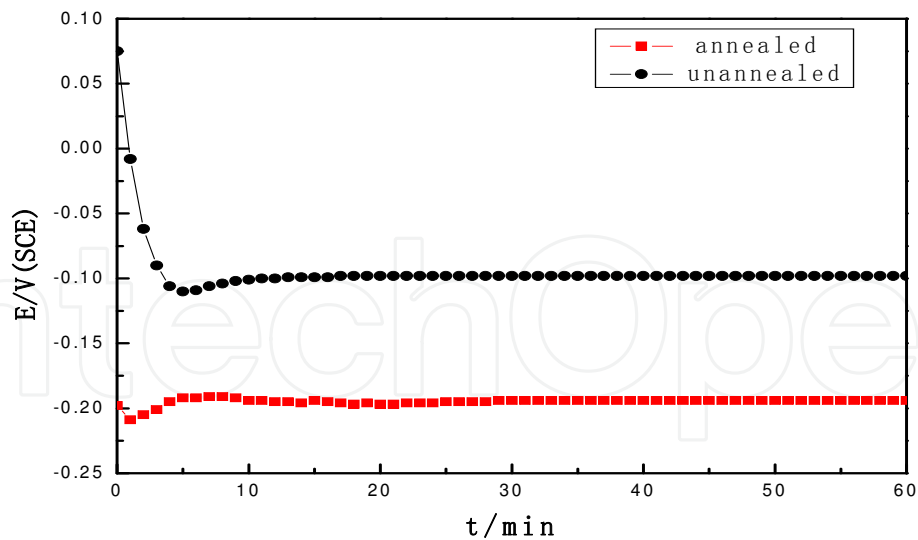


Fig. 1-25. The Corrosion potential change plotted as a function of time of annealed and unannealed samples in Hank's solution (PH7.45)

Figure 1-26 shows the polarization curves of the deposited samples at current density of  $5\text{mA}/\text{cm}^2$  before and after crystallization at  $450^\circ\text{C}$ . It can be seen from the polarization curves that the breakdown potential of the uncrystallized sample was  $1.3\text{V}$ , the current density in the process of polarization always was lower than that of the crystallized sample, and a longer passivation region emerging illustrates that the deposited sample at current density of  $5\text{mA}/\text{cm}^2$  before crystallization presented a better corrosion resistance in Hank's solution of PH7.45. Due to the single structure of unannealed Ti-O film, it is easy for the crystallized sample to arise more crystal defects, and bring about the crystal structure not unitary, thus presenting a poor corrosion resistance. From the cathodic-polarization curves of view, the slope of the sample's cathodic-polarization curves before crystallization was larger, but the current density was lower than that of the crystallized sample, thus presenting a better cathodic-polarization property.

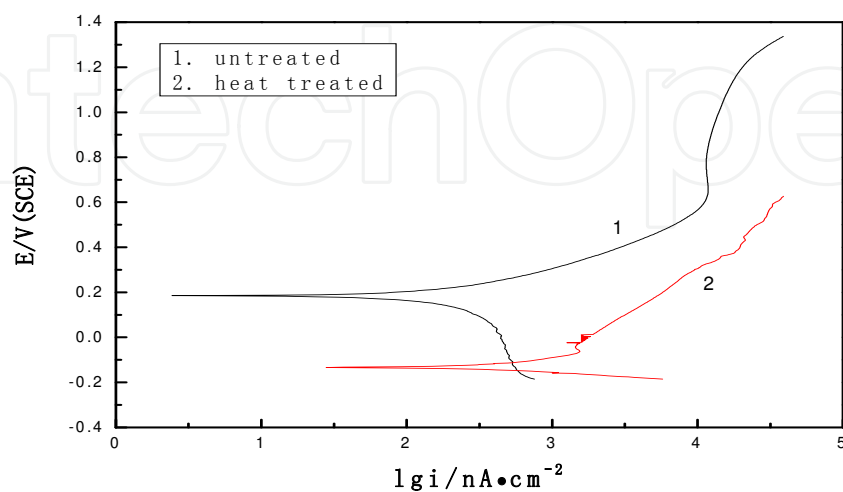


Fig. 1-26. The anodic-polarization curves of annealed and unannealed samples in Hank's solution (PH7.45)

Figure 1-27 shows the corrosion potential-time curves of the cathodically-electrodeposited TiNi SMA samples before and after crystallization at 450°C in Fusayama solution of PH6.13. It can be seen from the anodic-polarization curves that the stable corrosion potential of uncrystallized sample was more positive relatively, about -0.12V, but that of the crystallized one was more negative. That illustrates that the uncrystallized sample in Fusayama solution of PH6.13 possessed similarly a better thermodynamic stability.

Figure 1-28 shows the polarization curves of cathodically-electrodeposited TiNi SMA samples before and after crystallization at 450°C in Fusayama solution of PH6.13. It can be seen from the anodic-polarization curves that at lower potential, the crystallized sample's in the process of anodic-polarization was lower than the uncrystallized one's, but the uncrystallized sample's passivation region was shorter, from 0.5V to 0.7V, with a 200mV span. On the other hand, the passivation region of uncrystallized one was very long, from 0.4V to 1.3V, with a 900mV span. It can also be seen that the passivated film of crystallized sample began to breakdown from 0.8V, its current density increased quickly and far away exceeded that of the uncrystallized one. The sample before crystallization was still in a passive state, until 1.3V, the current density began to increase apparently, and its breakdown potential was 500mV higher than that of crystallized sample, presenting a better property of anti-corrosion. Similarly, this is because of that the crystal defects caused by crystallization brought about the drop of the property of anti-corrosion. From the cathodic-polarization curves of view, the uncrystallized sample similarly presented a better cathodic-polarization property.

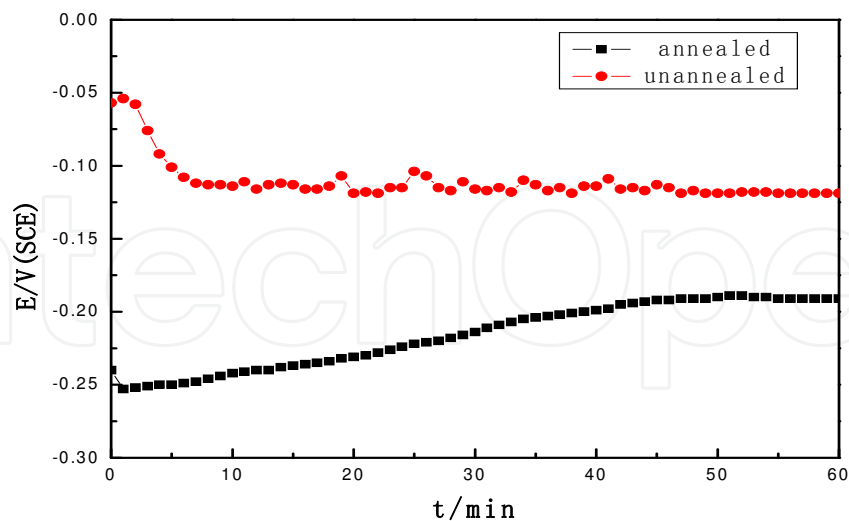


Fig. 1-27. The Corrosion potential change plotted as a function of time of annealed and unannealed samples in Fusayama solution (PH6.13)

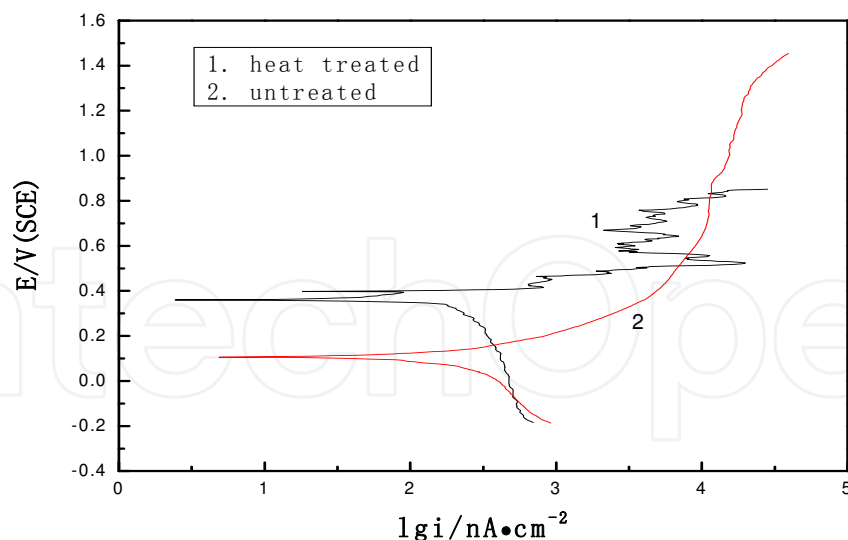


Fig. 1-28. The anodic-polarization curves of annealed and unannealed samples in Fusayama solution (PH6.13)

### 1.3.7 Effect of cathodic-electrodeposition time on surface morphology

Figure 1-29 shows the optical microscope morphologies of the cathodically-electrodeposited samples at current density of  $20\text{mA}/\text{cm}^2$  for different times. It can be seen from the figure that after deposited for 3min, obviously the Ti-O film began to emerge on the surface of TiNi SMA, fine, close and even, but there were some holes, which might be caused by the gas produced on the sample surface when cathodically-electrodeposited at the high current density. After deposited for 5min, the film thickness of the sample surface got increased apparently, but there were some big cracks emerging, adhered lumpily on the sample surface. After deposited for 7min, the Ti-O film fluffily adhered to the sample surface, bonding closely, with less cracks relatively, but uneven. The difference between the morphology of the sample deposited for 9min and that of the one for 7min was not great, fluffily adhered to the sample surface the same. Apparently, the surface of the sample deposited for 2h was different from that of the ones for short times, and its surface had no thicker fluffy Ti-O film, but with some holes. Similarly, the sample deposited for 12h had no fluffy Ti-O film emerging on the surface, but with some small cracks and porosities in different sizes and deepnesses. This is because of that at beginning of depositing, the Ti-O film nucleated and grew quickly on the sample surface, and its thickness increased quickly too. At the same time, with the increase of the thickness in the process of nucleation and growth, the Ti-O film on TiNi SMA surface continuously dissolved and peeled off, besides a lot of gas produced on the sample surface, that brought about uneven stress emerging internal Ti-O film, thus causing distributing lumpily. Because current density was higher, Ti-O film continuously formed and peeled off with time, thus gradually forming the fluffy distribution, and uneven very much. When to a certain time, because of reduction of  $\text{Ti}^{4+}$  in electrolyte, that made the level of Ti-O film peeling off far higher than that of forming, until the fluffy film disappearing completely, so some porosities in different sizes and deepnesses emerging. The cracks emerged in figure 1-27f might be caused by long time depositing, when drying, under the uneven stress, thus producing cracks. In short, at current density of  $20\text{mA}/\text{cm}^2$ , Ti-O film was a growth process of "thickening-cracking-lumping-peeling off-cracking again".

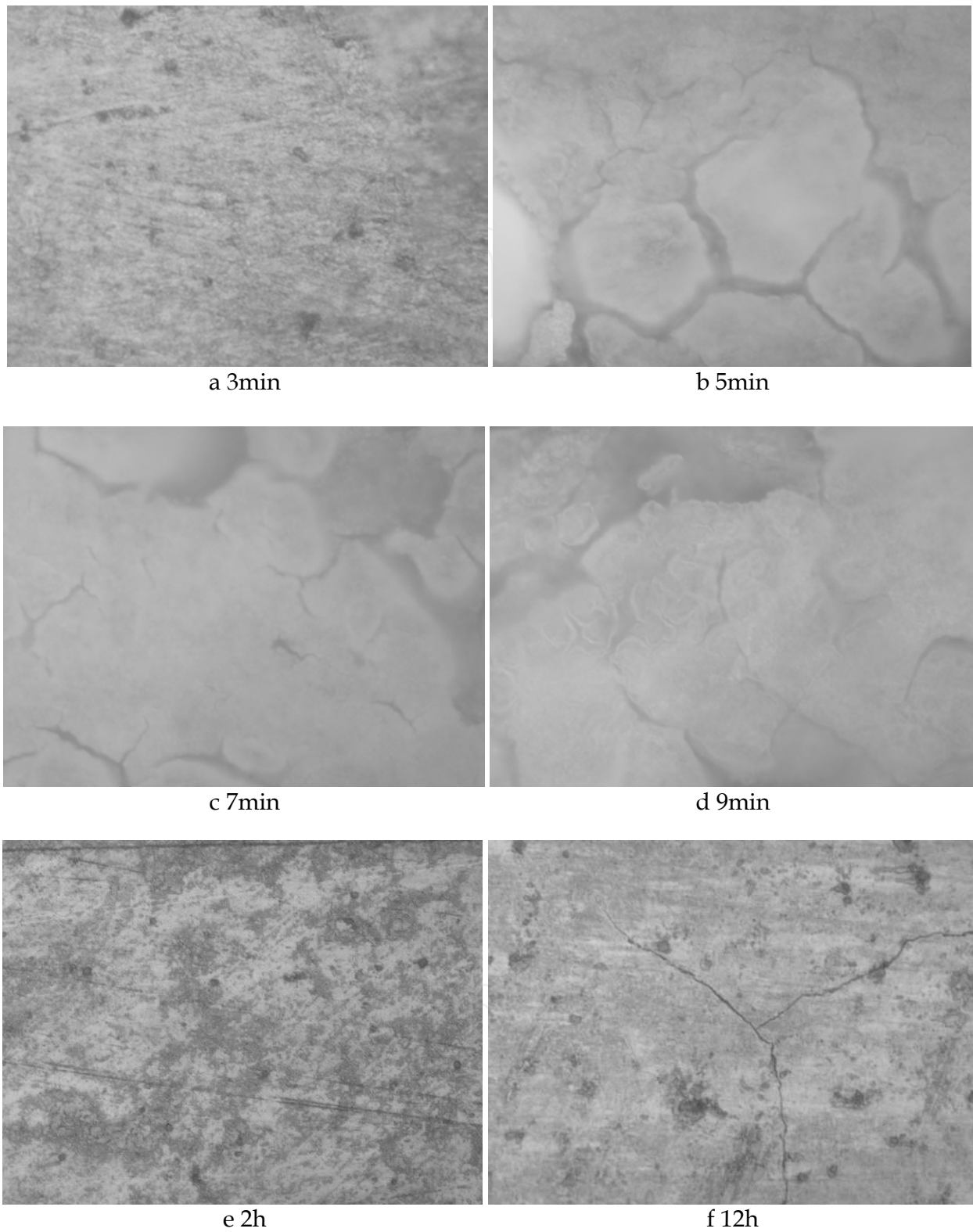
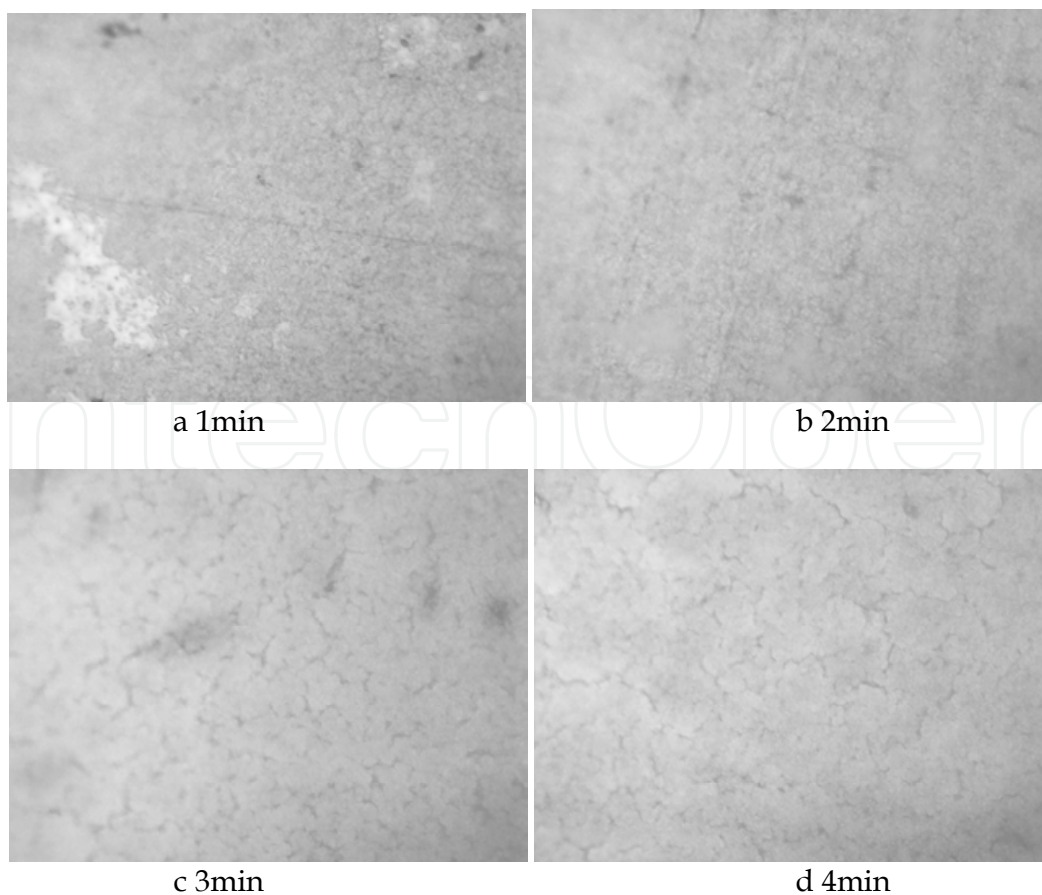


Fig. 1-29. Optical microscope result of sample by current 20mA/cm<sup>2</sup> for different times (1000×)

Figure 1-30 shows the optical microscope morphologies of cathodic-electrodeposition at low current density (5mA/cm<sup>2</sup>) for different times. It can be seen from the figure that at low current density, the Ti-O film deposited on the sample surface for 1min had formed in large

area, but not even, there were some places where undeposited or deposited very thin. The surface Ti-O film of the sample deposited for 2min had been very even, and adhered to the substrate's surface in large area. The surface Ti-O film of the sample deposited for 3min got thickening, distributed well laminally, there were a lot of fine holes and cracks in disorder. On the surface of the sample deposited for 4min, the lamina Ti-O film(s) combined and grew with each other, that made the holes number reduce, and fine cracks in disorder get long. Deposited for 5min, surface Ti-O film(s) continuously combined with each other, and thickened, with long surface cracks, Ti-O film adhered in large laminae to substrate surface. The surface Ti-O film of the sample deposited for 6min continued to thicken, and emerge big cracks and distributed not well lumpily on the substrate's surface. The big cracks in the Ti-O film of the sample deposited for 7min began to get less, fine and shallow, and there were some fine cracks emerging within the Ti-O film in big lumps. The surface cracks of the sample deposited for 8min got more and fine, and Ti-O film in big lumps got smaller. The surface Ti-O film of the sample deposited for 30min distributed well on the substrate surface in fine particles was big relatively. From the change of the surface morphology of Ti-O film in the figure of view, that was a process of "forming-evening-cracking-aggregating-cracking again". It can be seen that the particles of sample cathodically-electrodeposited at low current density were fine and even. This is because of that the drying force for nucleation of Ti-O film at low current density was not so great, the film would slowly nucleate on the substrate surface, besides at low current density, the gas produced on the sample surface was not strongly, so that made the Ti-O film adhere evenly to the substrate surface. Among the samples, the Ti-O film of the sample deposited at 5mA/cm<sup>2</sup> for 4min had the best levels of evenness and thickness.



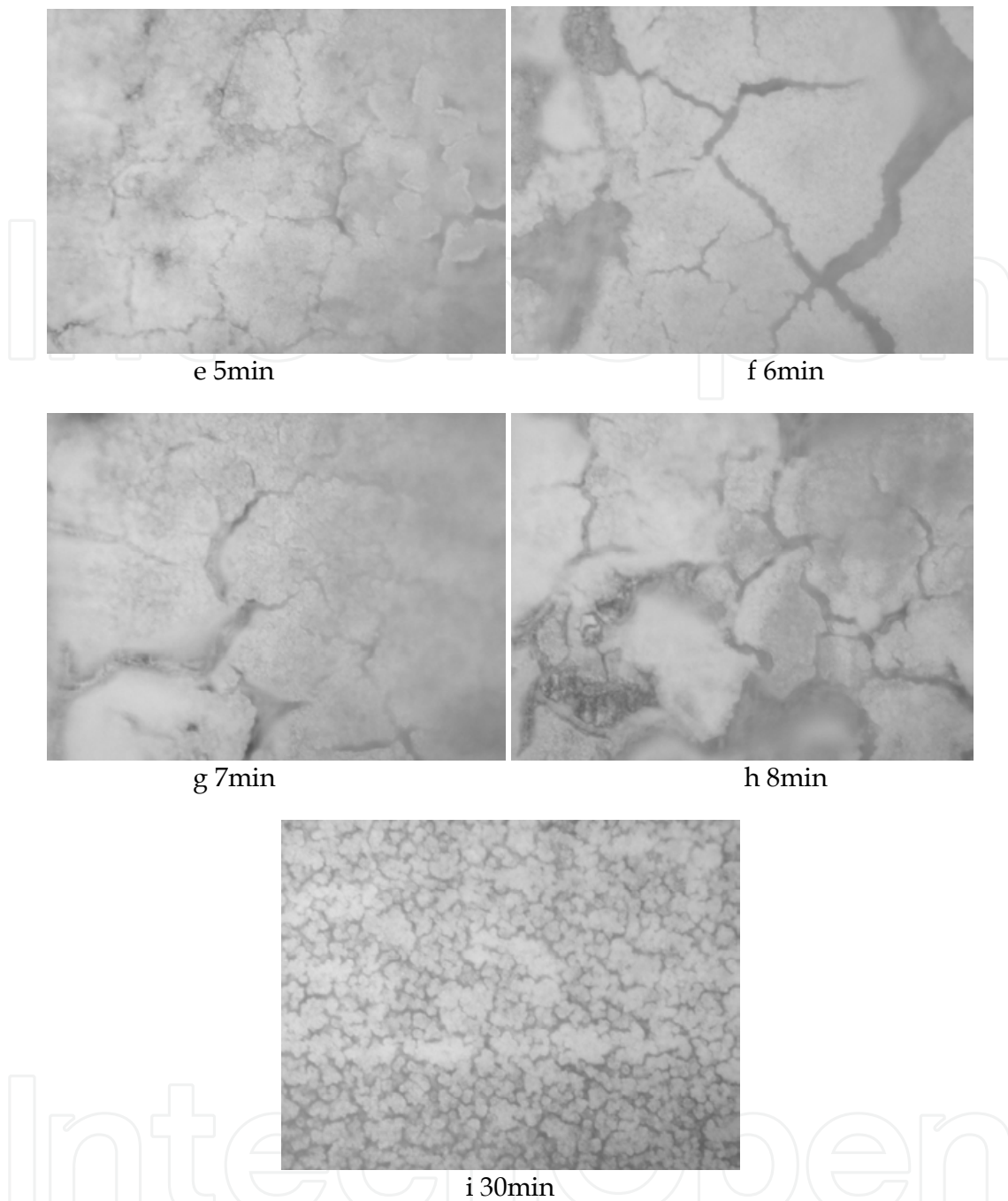


Fig. 1-30. Optical microscope result of samples by current  $5\text{mA}/\text{cm}^2$  for different times ( $1000\times$ )

### 1.3.8 Effect of electrolyte PH value and $\text{NO}_3^-$ concentration on cathodic-electrodeposition

Figure 1-31 and table 1-2 are the optical microscope morphologies, technical parameters and results affected by cathodic-electrodeposition in different PH values of electrolyte and  $\text{NO}_3^-$  concentrations. It can be seen from the figure 1-29a that there was no obvious Ti-O film existing on the sample surface. This is because of that acidity of the solution was too high, although  $\text{OH}^-$  produced on the cathodic sample surface, then quickly dissolved, it did not form a Ti gel to adhere to the sample surface within a short time. It can be seen from figure 1-29b

that there was an obvious Ti-O film produced. This because of that when PH value increased, Ti gel could be formed within a short time. It can be seen from figure 1-29c that there was less Ti-O film formed. This is because of that under the circumstance of higher PH value, although there was no  $\text{NO}_3^-$  reduced to  $\text{OH}^-$  yet, at driving of high current density,  $\text{H}_2\text{O}$  was reduced to  $\text{OH}^-$  which could form less Ti gel within a short time. But at low current density, even if small amount of  $\text{NO}_3^-$  was added in, it was not enough to form a Ti gel within a shorter time, this can be seen from figure 1-29d and e. It can be seen from figure 1-29e that under higher PH value, adding in enough  $\text{NO}_3^-$ , it could form fine and close Ti-O film at low current density within a shorter time. So, electrolyte PH value and  $\text{NO}_3^-$  concentration have played a vital role in the process of TiNi SMA cathodic-electrodeposition.

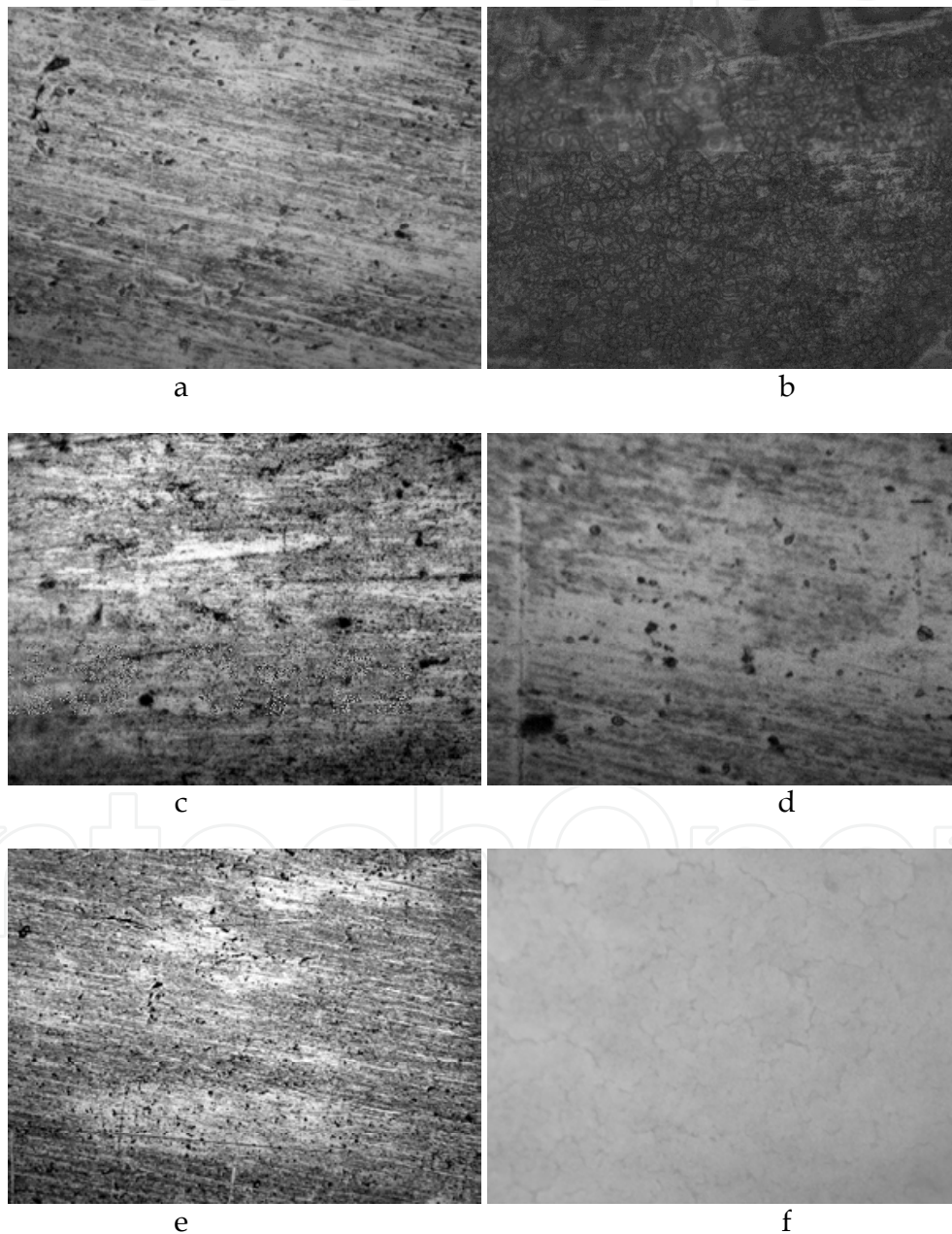


Fig. 1-31. Optical microscope of sample in electrolyte of different PH value and  $\text{NO}_3^-$  concentration (1000 $\times$ )

Picture	PH	NO <sub>3</sub> <sup>-</sup> (M)	i(mA/cm <sup>2</sup> )	t(min)	Result
a	0.71	0.02	20	4	No film
b	1.2	0.02	20	4	Thick film
c	1.2	0	20	4	Thin film
d	1.2	0	5	4	No film
e	1.2	0.02	5	4	No film
f	1.2	0.2	5	4	Thick film

Table 1-2. Processing parameter and electrodeposition result in electrolyte of different PH values and NO<sub>3</sub><sup>-</sup> concentrations

#### 1.4 The summary of this chapter

1. In self-prepared Ti(SO<sub>4</sub>)<sub>2</sub> solution of electrolyte (PH1.2), at a constant current density of 5mA/cm<sup>2</sup>, cathodically-electrodeposited for 4min, a layer of amorphous Ti-O film could be obtained on TiNi SMA. This Ti-O film is composed of a lot of fine and close particles gathered, the particles' size in dozens of nanometers. And the atomic ratio of Ti and Ni reached to 3:1 through a primary detection by EDS. This illustrates that there were a lot of Ti element included in the film, and this closely bonding of fine particles has contributed to strengthening the surface properties of TiNi SMA.
2. Through XPS analysis, Ti-O film elements of TiNi SMA cathodically-electrodeposited existed in form of TiO<sub>2</sub> or hydrate Ti(OH)<sub>4</sub>.
3. After the sample cathodically-electrodeposited Ti-O film was crystallized at 300°C, no TiO<sub>2</sub> existing was found, but crystallized at 450°C, there was anatase TiO<sub>2</sub> peak emerging. After the non-deposited blank TiNi SMA sample was crystallized at 450°C, there was no TiO<sub>2</sub> peak emerging. This illustrates that the film obtained by cathodic-electrodeposition was certainly an amorphous Ti-O film, and its composition was existed in form of hydrate Ti(OH)<sub>4</sub>.
4. The tests of corrosion potential and electrochemical corrosion illustrated that the TiNi SMA cathodically-electrodeposited presented the better thermodynamic stability and corrosion resistance in Hank's solution (PH7.45) and Fusayama solution (PH6.13).
5. At different current densities, there was much different in roughness, even level, thickness and crack of Ti-O film surface morphology of cathodically-electrodeposited TiNi SMA, among them, the film obtained at the current density of 5mA/cm<sup>2</sup> was the best one.
6. The thermodynamic stability and electrochemical anti-corrosion of the cathodically-electrodeposited samples at different current densities in Hank's solution (PH7.45) and Fusayama solution (PH6.13) were different. Those of the sample deposited at current density of 20mA/cm<sup>2</sup> were better. But for the one crystallized at 450°C, and cathodically-electrodeposited at the current density of 5mA/cm<sup>2</sup>, its thermodynamic stability and electrochemical anti-corrosion were better.
7. The surface morphologies of Ti-O film before and after crystallization at 450°C were different. The crystallized Ti-O film was distributed in fine and close particles. Moreover the sample before crystallization had better thermodynamic stability and corrosion resistance in Hank's solution (PH7.45) and Fusayama solution (PH6.13).
8. The morphologies of the Ti-O film(s) obtained which were cathodically-electrodeposited for different times were different. At the current density of 20mA/cm<sup>2</sup>, The Ti-O film change with time was a growth process of "thickening-cracking-

agglomerating-peel off-cracking again". At that of  $5\text{mA}/\text{cm}^2$ , the change was a process of "forming-evening-cracking-agglomerating-cracking again".

9. The electrolyte's PH value and  $\text{NO}_3^-$  concentration played a vital role in the process of TiNi SMA cathodic-electrodeposition. Only under PH1-3 and about 0.2M of  $\text{NO}_3^-$  concentration, a better effectiveness of cathodic-electrodeposition could be obtained.

## 2. Chapter II

### 2.1 Preface

The key, for a plant material to bonding surface, is that the material must be with excellent bioactivity, that is, the biomaterial should have capability of closely bonding with surrounding living tissue under physiological fluid environment<sup>[9]</sup>. The bioactive bonding called, is that after a bone plant is planted into human body, there will be a layer of bioactive hydroxyapatite (HA) forming on the material's surface. HA is a main inorganic substance, occupying about 69%, and about 41.8% in volumetric fraction of human bone. Through HA thin layer, chemical bonding at a molecular level is formed. After planting into human body for 3-6 months, the interface strength of the bioactive bonding is equal to or higher than that of surrounding bone tissue<sup>[9]</sup>. Under the circumstance of guaranteeing other properties, promoting coating's bioactivity will be helpful to shorten osseointegration period, make patient's injured site(s) recover the functions early, and alleviate suffering<sup>[10]</sup>.

Blood compatibility includes quite wide content. There are the reactions at cell level, such as thrombosis (platelet adhesiveness, agglomerating, and deformation) when connecting with material, haemolysis and leucopenia; there are the reactions at plasma protein level, such as coagulation system and fibrinolytic system activation; and there are the reactions at molecular level, such as immune ingredient change, platelet receptor and ADP (adenosine diphosphate)<sup>[11]</sup>.

When a material connects to blood, a competitive protein adsorption will come about first to form a complex protein adsorption layer, then blood cell and platelet adhesiveness, and then thrombosis, if which can not be repaired or cured, it is easy to bring about coagulating. So, avoiding thrombosis and preventing coagulation are the most important factors of a biomaterial's blood compatibility. Approach a mechanism of thrombosis to promote material's blood compatibility is a research hot point in the academic circle<sup>[12,13]</sup>, and it has been made a great progress recent years.

In this chapter, evaluations for the biomaterials' blood compatibility in vitro have been experimentally carried out in following two aspects<sup>[14]</sup>:

1. Haemolysis rate test For a plant apparatus directly connected to blood, it is necessary to carry out the experiment on haemolysis rate in vitro. Under normal circumstance, the average life of erythrocyte is 120d. Under the same reason, the life of erythrocyte shortens, it is called that a haemolysis process comes about. Through haemolysis rate experiment the rank of toxicity produced by erythrocyte in blood connecting to material can be evaluated, the erythrocyte in blood will be damaged in varying degrees because of the toxic substance(s) of the material, to release hemoglobin, and to bring about haemolysis. By testing the amount of hemoglobin released from the material, the haemolysis rate for the material can be obtained. Generally speaking, the concentration

of a toxic substance which can produce haemolysis reaction is higher than that of the one which can only produce toxic effect. For the biomedical materials, it is extremely important to alleviate erythrocyte damage.

2. Dynamic coagulation time test Blood would be activated to coagulate and to affect platelet's formation and function as a material connects with blood. And blood coagulation is a result from a series of reaction in blood. There are two processes which would initiate coagulation, that is, intrinsic coagulation (activated by coagulation factor XII) and extrinsic coagulation reactions. Firstly, prothrombin factor XII was changed into active factor XII a; the active XIIa made the coagulation factor XI change into an activation factor XIa, and furthermore made factor IX activate to be IXa; then the activated IXa combined with the factor VIII, phosphatide and  $C^{2+}$  ions to form a complex compound, which would make factor X change into activation factor Xa; furthermore, the active factor Xa combined with factor Va, phosphatide and  $C^{2+}$  to form the complex compound which would make prothrombin change into thrombin; finally, the thrombin made fibrinogen molecules change into fibrinogen monomer, then into the fibrin colloid under the action of activated factor XIII a, thus forming the blood clots. On the other hand, the extrinsic clotting system, activated by tissue factor and VII factor, directly made the factor X activate to be Xa, the next process emerged was as the same as the intrinsic one's<sup>[15]</sup>.

The process of blood coagulation shows that globin and fibrin in blood on material's surface would bring about activation of the coagulation factor, thus causing fibrin to form and to coagulate. At the same connecting time, by the experiment of dynamic coagulation time in vitro, the activation degrees of different materials on intrinsic coagulation factor can be compared. The activation degrees on coagulation are different, so are the coagulation degrees. With the time of material connecting to blood, coagulation degrees increases correspondingly. The dynamic coagulation time curve is a relation curve to absorbance and time. The more smooth the curve is, the longer the coagulation time lasts, it shows, and the lower the degree activated by coagulation is. And the longer the coagulation time lasts, it shows, the lower the degree for a material to bring about thrombus is, and the better the material's anti-coagulating property is.

## 2.2 Experimental methods

### 2.2.1 Experimental materials and media

The experimental materials were the examples of TiNi SMA, TiNi SMA after anodic-oxidation and TiNi SMA after cathodic-electrodeposition respectively. The size of all the samples was in 10mm×10mm×1mm.

SBF (Simulated body fluid) solution<sup>[16]</sup> (making up to PH7.40 with diluted hydrochloric acid and NaOH solution)<sup>[17]</sup> and fresh blood of New Zealand rabbit.

SBF solution ingredient:  $Na_2SO_4$  0.07g +  $Na_2HPO_4$  0.36g +  $NaHCO_3$  0.35g + NaCl 7.88g + KCl 0.37g +  $MgCl_2$  0.31 +  $CaCl_2$  0.28g +  $H_2O$  1L.

### 2.2.2 Experimental methods

#### 2.2.2.1 Evaluation of biocompatibility of TiNi SMA surfacely-modified

The samples before and after anodic-oxidation respectively were dipped into 25ml SBF solution of PH7.40. The working area was 10mm×10mm, and the non-working one was

coated with silica gel. Dipping for 7d in a water bath at 37°C. The deposition of the Ca/P layer on the surface was detected with Finder 1000 type of EDS.

The samples before and after cathodic-electrodeposition respectively were dipped into 25ml SBF solution of PH7.40. The working area was 10mm×10mm, and the non-working one was coated with silica gel. Dipping for 7d in a water bath at 37°C±1°C, the solution was changed every two days. The deposition of the Ca/P layer on the surface was detected with Finder 1000 type of EDS. And the hydroxyapatite (HA) on the surface was analyzed with D/max 2000type of X-ray diffractometer (XRD).

### 2.2.2.2 Test of hemolysis rate of TiNi SMA after surfacely- modified

8ml fresh rabbit blood selected was anti-coagulated with 1ml heparin solution, and diluted with 10ml physiological saline. The samples were put in 10ml physiological saline in the water bath at 37°C, then putting in 0.2ml dilution blood, mixing well gently, and continuing to keep the temperature for 60min. Then the fluid was poured into a test tube, separated at a speed of 1000r/min with LXJ-64-01 type of separator, and the up layer solution was taken out to test absorbance value at wave length of 545nm with Lambda 35 type of spectrophotometer. Anode control group used 10ml distilled water + 0.2ml dilution blood, and cathode one 10ml physiological saline + 0.2ml dilution blood. By the formula:

$$\alpha(\%) = \frac{D_t - D_{nc}}{D_{pc} - D_{nc}} \times 100\% \quad (2.1)$$

$D_t$  : Sample absorbance;  $D_{nc}$  : Cathode control group absorbance;  $D_{pc}$  : Anode control group absorbance hemolysis rate was taken out.

### 2.2.2.3 Test of dynamic coagulation time of TiNi SMA after surface modification

1. To compound an ACD blood and 0.47g citric acid, 0.3g glucose and 1.22g sodium citrate were dissolved in 100ml distilled water to compound the blood preservation solution (ACD). Taking that fresh rabbit blood : ACD as 1 : 4 in proportion to compound ACD blood.
2. Taking 0.2ml ACD blood and dropping on the surface of the test material after clearing. Adding to 20μl from the 0.2ml CaCl<sub>2</sub> solution, then mixing well and then recording time.
3. At 5, 10, 20, 30, 40, 50 and 60min of given times, respectively having 100ml distilled water flowed through the material surface slowly, the fluid was gathered up to a beaker, the absorbance values (O. D.) of the solution at different times were got at 540nm wavelength with Lambda 35 type of spectrophotometer, and plotting the O. D.-t curves to compare. Taking the connecting time at 0.100 absorbance as the dynamic coagulation time for different materials.

## 2.3 Experimental results and discussion

### 2.3.1 Evaluation of biocompatibility of TiNi SMA surfacely-modified

Figure 2-1 shows the EDS results of Ca/P deposition on TiNi SMA before and after anodic-oxidation respectively in SBF solution for 7d. It is seen from Figure 2-1a that there was small

amount of the elements of Ca, P and O on the sample before oxidation, this coincides with the Hanawa's investigation<sup>[18]</sup>. But there was a lot of the elements of Ca, P and O on the sample after oxidation, as shown in figure 2-1b.

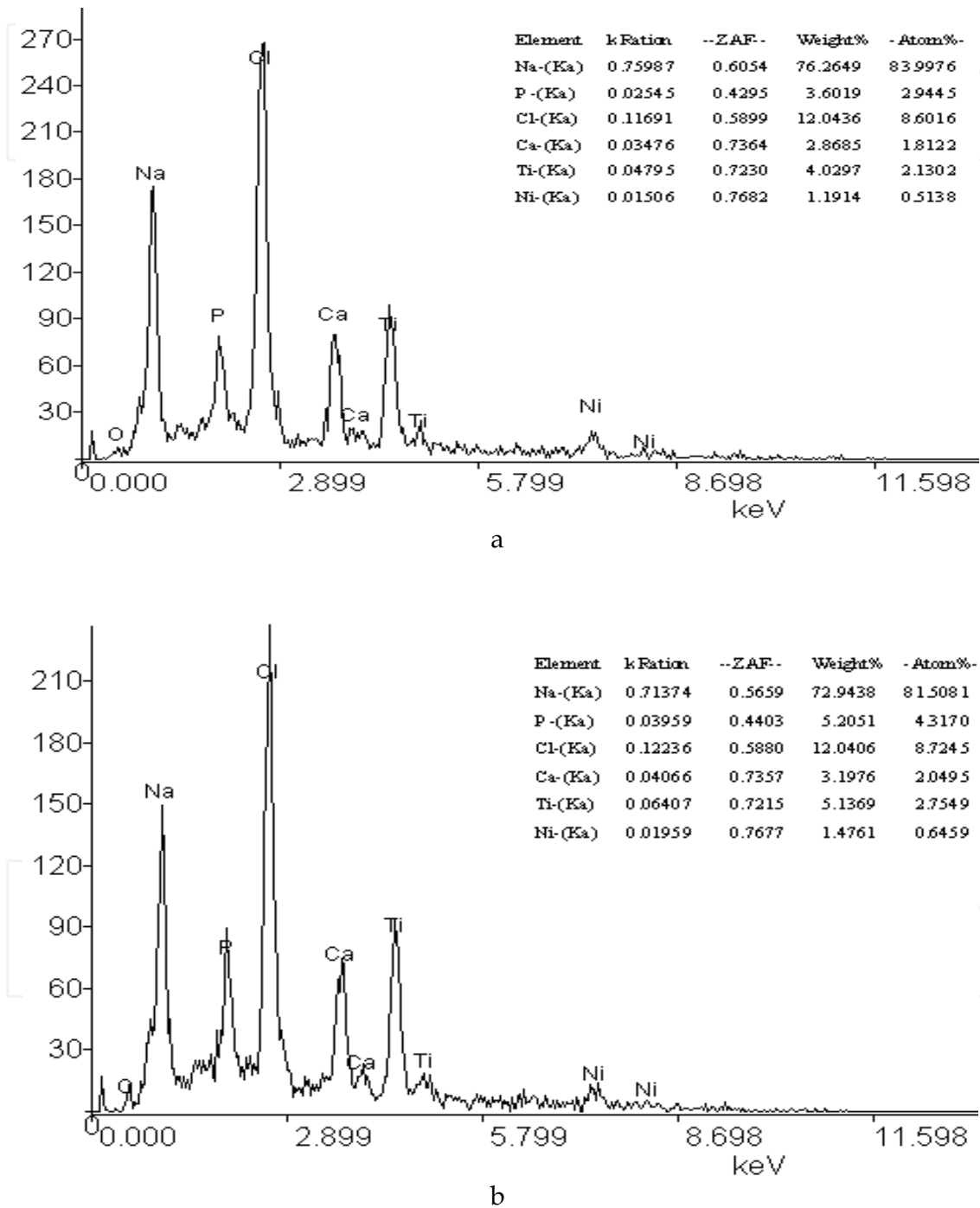
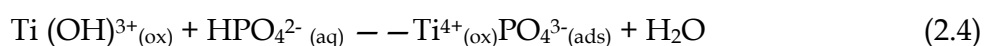


Fig. 2-1. EDS result of Ca/P coating in SBF solution (PH7.40) (a TiNi SMA; b anodic-oxidation)

This is because of that Titanium dioxide's isoelectric point has a great influence on the behavior of Titanium in organism, the isoelectric point of  $\text{TiO}_2$  is about 6.2<sup>[19]</sup>, which is somewhat lower than PH value (7.4) in physiological environment. This illustrates that under physiological environment, the Titanium surface may be with some weak negative charges. And this kind of surface with negative charges has a close relation to osseous integration between plant and its peripheral live bone<sup>[20-23]</sup>. In the body fluid,  $\text{Ca}^{2+}$  will combine with the negative charge on the  $\text{TiO}_2$  surface under the action of Coulomb force. And the  $\text{OH}^-$  on the surface will adsorb  $\text{PO}_4^{3-}$  through hydrogen bond to gather forward to surface, thus it can introduce calcium phosphorus layer to deposit on the surface. The concrete adsorption process is as following:

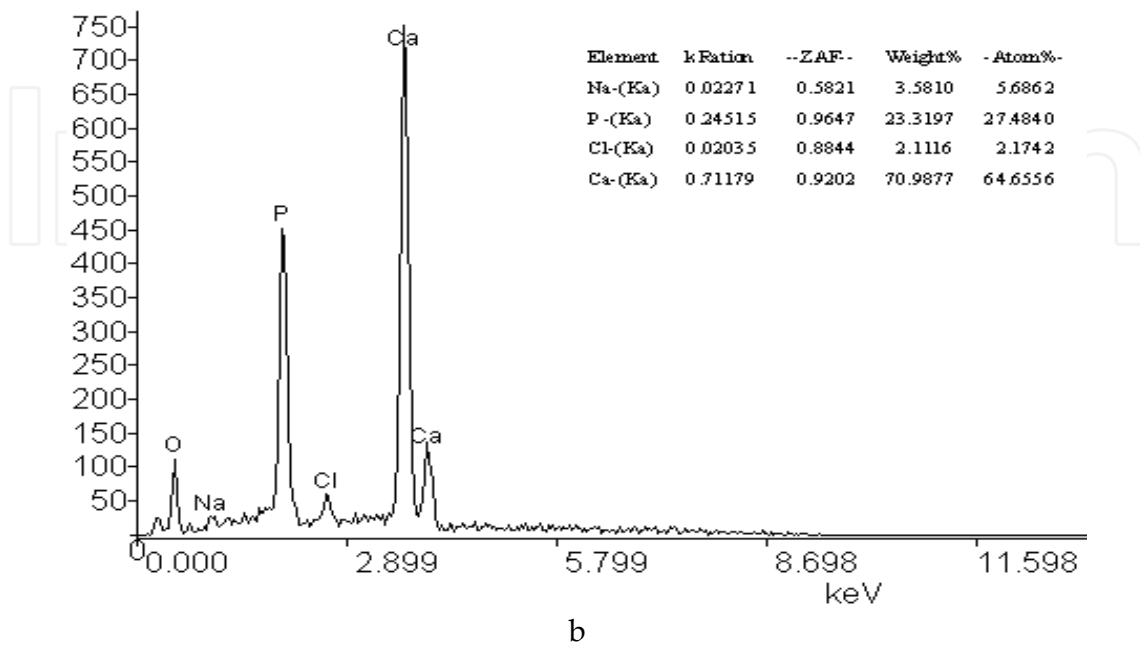
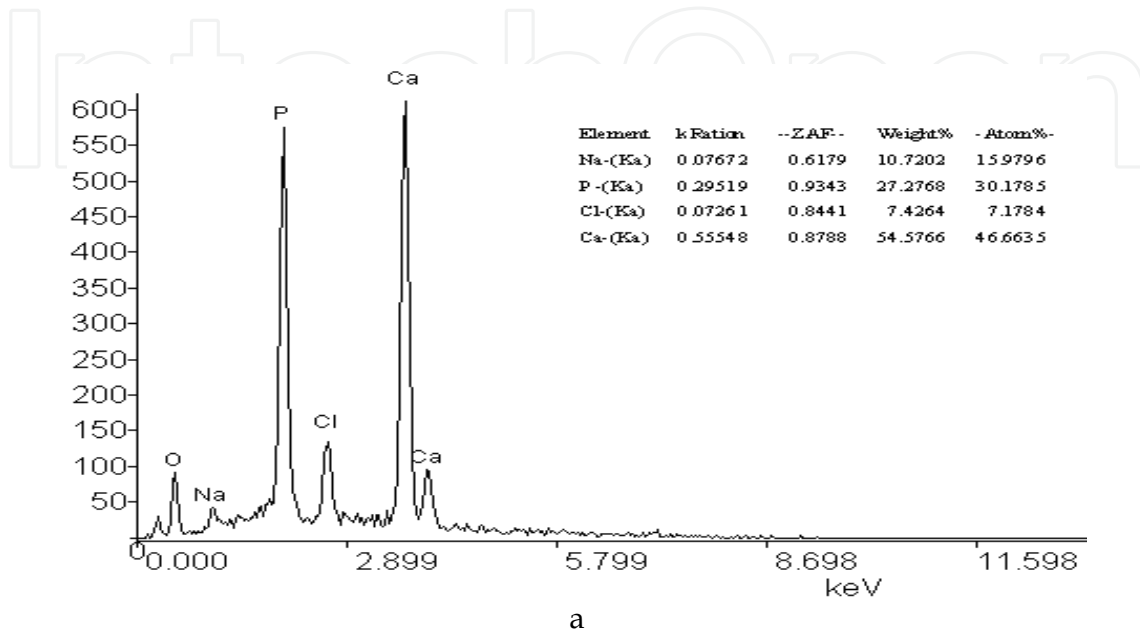


Among them, (ads), (ox) and (aq) respectively stand for ions adsorbed on the alloy surface, substances in oxidation layer and ions in solution.

The self-produced oxidation film of TiNi SMA is too thin, not stable, but the  $\text{TiO}_2$  film produced by anodic-oxidation is thicker, so the capability to adsorb Ca/P layer is stronger. This illustrates that anodic-oxidized TiNi SMA may have some bioactivity, but it needs further verification.

Figure 2-2 shows an EDS result of Ca/P deposition in SBF solution of TiNi SMA before and after cathodic-electrodeposition. It can be seen from the figure that after dipping for 7d, there were higher contents of Ca and P elements deposited on the sample surface. Ca and P mole ratio reached to 1.5 : 1 in figure 2-2a; 2.4 : 1 in figure 2-2b; and 1.8 : 1 in figure 2-2c. The material's after cathodic-electrodeposition is the highest, the one's crystallized came second and the un-treated sample's was the lowest. This is because of, that the Ti-O film obtained after cathodic-electrodeposition was mainly  $\text{Ti}(\text{OH})_4$ , because of  $\text{OH}^-$  existence, it was easy for apatite on the surface to nucleate. Li et al<sup>[24]</sup> found in research for bioactivity of titanium metals that the surface titanium oxide layer including Ti-OH group as well as being with electronegativity was one of the major factors to introduce HA nucleation. Because  $\text{HPO}_4^{2-}$  and  $\text{PO}_4^{3-}$  generally exist more easily under alkaline environment, crystallization treatment cause  $\text{OH}^-$  loss, so nucleation is comparatively more difficult. There are researchs showing that the materials with high mole ratio are more stable than ones with low mole ratio under physiological environment. High Ca and P mole ratio is advantageous to prevent from host organization reaction of fast dissolution of small molecules after material planted and it can also prevent from the acute inflammation reaction caused due to fast degradation<sup>[25]</sup>.

At constant temperatures, solubility product of  $\text{Ca}_{10}(\text{PO}_4)(\text{OH})_2$  (hydroxyapatite, HA) is far less than that of other phosphates, so HA oversaturation in calcification solution at the same concentration is higher than that of other phosphates. It can be inferred that surface crystal may mainly be HA.



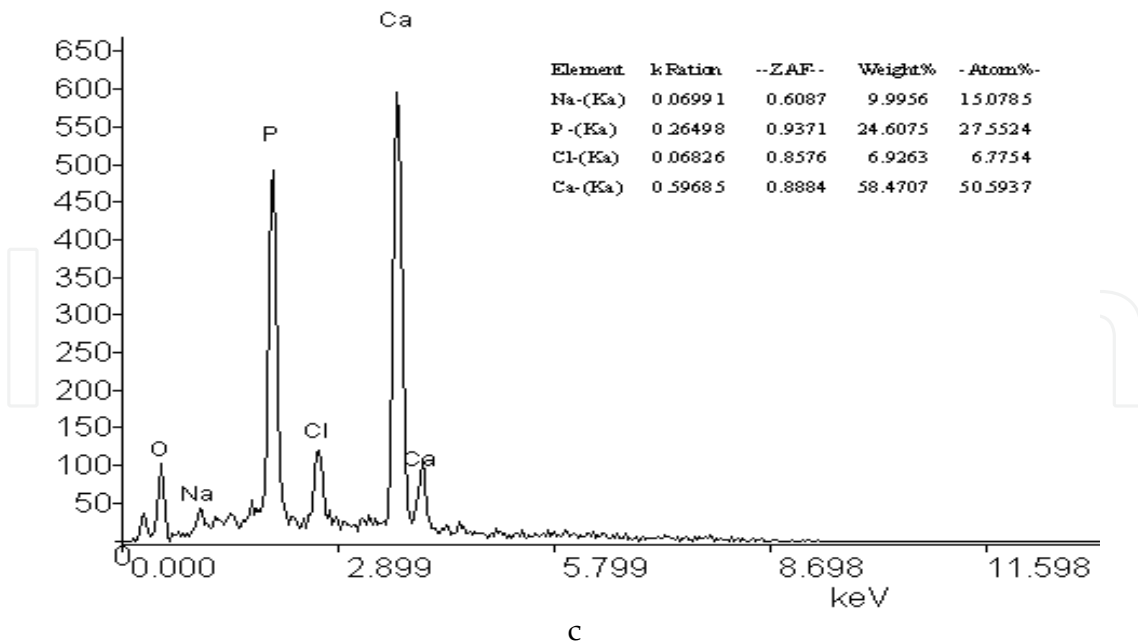


Fig. 2-2. EDS result of Ca/P coating in SBF solution (PH7.40) (a TiNi SMA; b electrodeposition; c annealed)

Figure 2-3 shows the surface XRD analysis results of cathodically-electrodeposited samples in SBF solution before and after crystallization respectively. It can be seen from the figure that HA existed on both samples. This illustrates when an amorphous Ti-O film riching in Ti-OH group was dipped in SBF solution for 7d, HA could form on the surface; this also illustrates that the obtained TiO<sub>2</sub> after crystallization treatment still preserved some hydroxyl groups with bioactivity. The formation process of hydroxyapatite on a material surface is actually a formation and growth one of a new phase. The process can be summarized with two stages<sup>[26]</sup>.

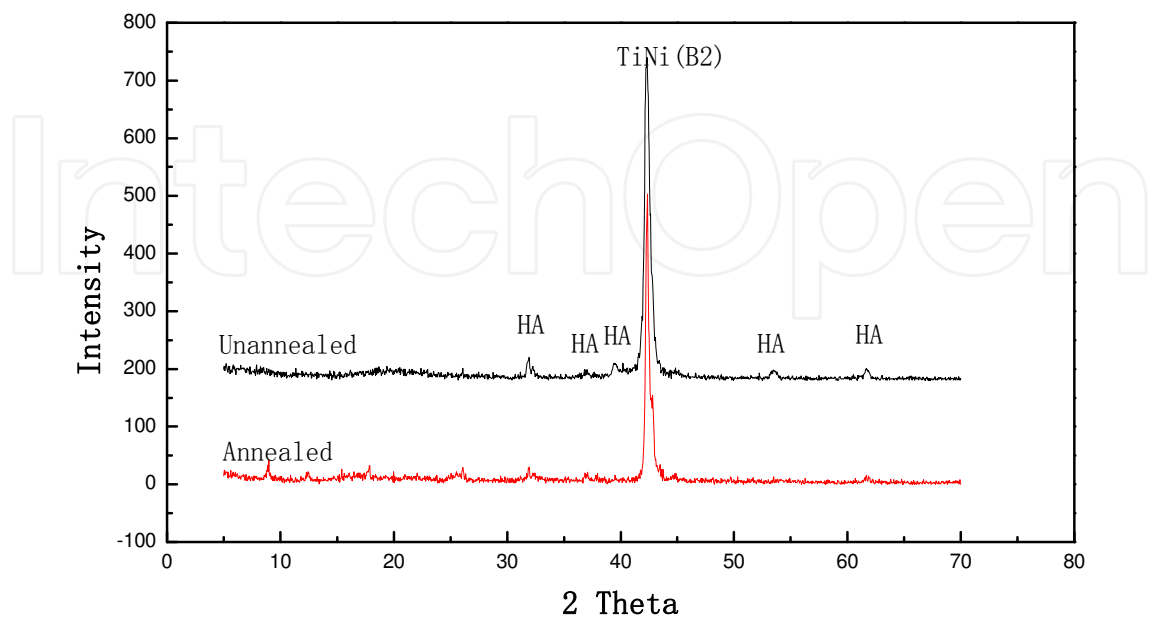


Fig. 2-3. XRD result of HA on the surface of sample cathodically-electrodeposited

### 2.3.1.1 Nucleation formation

When a material connects to SBF solution, because of electrostatic attraction,  $\text{Ca}^{2+}$ ,  $\text{HPO}_4^{2-}$  and  $\text{PO}_4^{3-}$  directly acting on solid surface are adsorbed on the surface, to form calcium-phosphorus compound, which interacts with  $\text{HPO}_4^{2-}$  and  $\text{CO}_3^{2-}$  in SBF solution, to form a new phase nucleus. According to two-dimension nucleation theory, as soon as a nucleus forms, the reactant ions will continuously nucleate on the deposited surface, and the crystal will continuously grow.

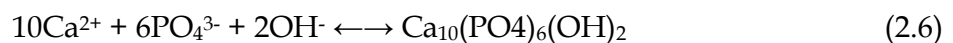
The factors to affect nucleation are those as following: ① Calcium-phosphorus concentration at localization on surface plays a very key role to nucleation. For a sample cathodically-electrodeposited, the particle distribution on the surface film makes surface roughness of the sample increase, and surface area increase too. Thus the concentration at localization on the surface would be comparatively higher than that on a smooth surface. So, under the same conditions, it is easier for  $\text{Ca}^{2+}$  and  $\text{HPO}_4^{2-}$  concentration on the roughness surface to reach the nucleation critical value. ② The interfacial energy of material surface. Apatite crystals form and directly grow on the material surface. It may be thought that is increasing ionic concentration in the saturated solution to form the low interfacial energy surface. According to Ostward's nucleation theory, the free energy to nucleate depends on solution's oversaturability (S), pure interfacial energy ( $\sigma$ ), temperature (T) and particle surface area (A):

$$\Delta G = -T \ln S + \sigma A \quad (2.5)$$

This nucleation theory illustrates that: the increase of solution's oversaturability and decrease of pure interfacial energy are advantageous to interface heterogeneous nucleation. S increasing, will make nucleation free energy decrease. As long as S is high enough, even if a surface with low energy, which has not been subjected to any treatment, it can also introduce heterogeneous nucleation. Because ionic concentration is high, it can overcome the barrier of material's surface nucleation, to nucleate on the surface. ③ The geometric morphology of material surface. It is reported that a crystal nucleus firstly occurred at the roughness places on a surface. Because higher localization concentration can be kept in these regions, the critical value to nucleate would quickly be reached, at the same time these locations supply the nucleation spots.

### 2.3.1.2 Growth of a crystal nucleus

In the process of hydroxyapatite formation, crystal nucleus formation is a homogeneous nucleation, that is, to form a nucleus on the certain substrate. Through the nucleation process, changes in crystal structure and composition accomplish simultaneously. A main role for grain boundaries to nucleate is to decrease boundaries' area and interface energy, thus to low the nucleation work. The decrease of interface energy drives crystal to grow. The deposition process of hydroxyapatite on sample surface in SBF solution is as following<sup>[27]</sup>:



As a consequence, HA begins to deposit on sample, as long as apatite crystal nuclei form, the nuclei will consume Ca and P in solution, hydroxyapatite continuously deposit on sample surface.

### 2.3.2 Haemolysis rate test of TiNi SMA after surface modification

When blood connects with a foreign material surface some red cells will be destroyed to release hemoglobin, that is, haemolysis occurring. A material with good blood compatibility should have a lower haemolysis rate. Figure 2-4 shows a haemolysis rate tested result of TiNi SMA samples, which were untreated, anodically-oxidized and cathodically-electrodeposited respectively. It can be seen that the TiNi SMA and its surface-modified materials have met the medical requirement (<5%) for a biomaterial. Haemolysis rate of the modified material has decreased somewhat. And haemolysis rate of anodically-oxidized sample was lower than that of cathodically-electrodeposited one. This is because of that,  $\text{TiO}_2$  crystals have a good blood compatibility. Besides, the material surface smoothness and film quality have effects on haemolysis rate. Haemolysis rate of cathodically-electrodeposited sample is higher than that of anodically-oxidized one. This is relevant to the smoothness differences on sample surface.

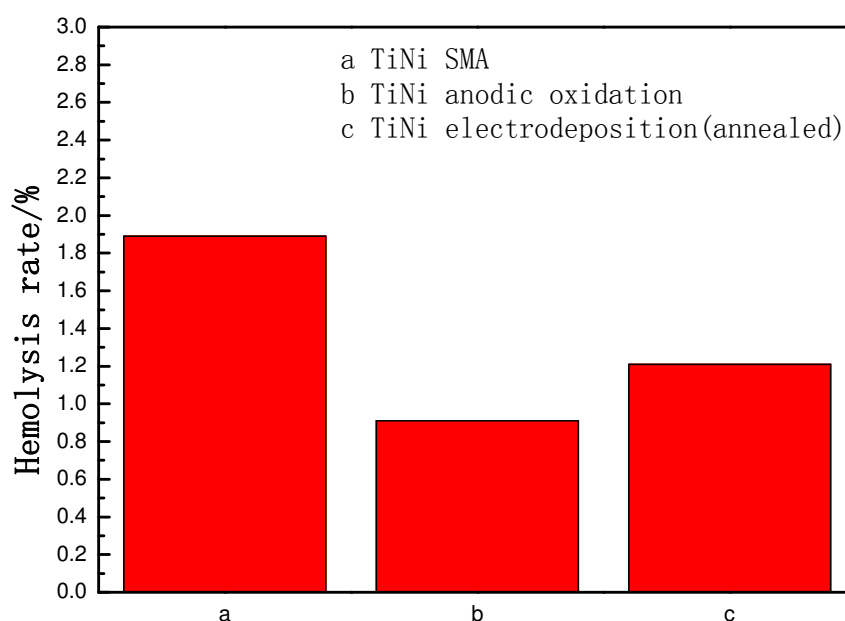


Fig. 2-4. Haemolysis rate of modified TiNi SMA

### 2.3.3 Dynamic coagulation time test of TiNi SMA after surface modification

The experiment on dynamic coagulation time is to test the degree of activating endogenous coagulation factor, the more smooth the dynamic coagulation curve is, the higher the absorbance at ordinate will be. This shows that, the longer the coagulation time, the lower the degree of activating coagulation factor. Generally, the time at O.D.=0.100 is often settled as the coagulation time, in order to comparing. Figure 2-5 shows the change curves of absorbance and blood connecting time of TiNi SMA, which were surface modified by anodically-oxidized and cathodically-electrodeposited respectively. It can be seen from the figure that the absorbance of the anodically-oxidized sample is highest, and the coagulation time is the longest. This illustrates that it has an excellent anti-coagulation property. The secondary is the cathodically-electrodeposited sample, and the last one is TiNi SMA sample (un-treated). Besides, material surface smoothness also has an effect on dynamic coagulation time. Generally the higher the surface smoothness, the longer the dynamic coagulation time.

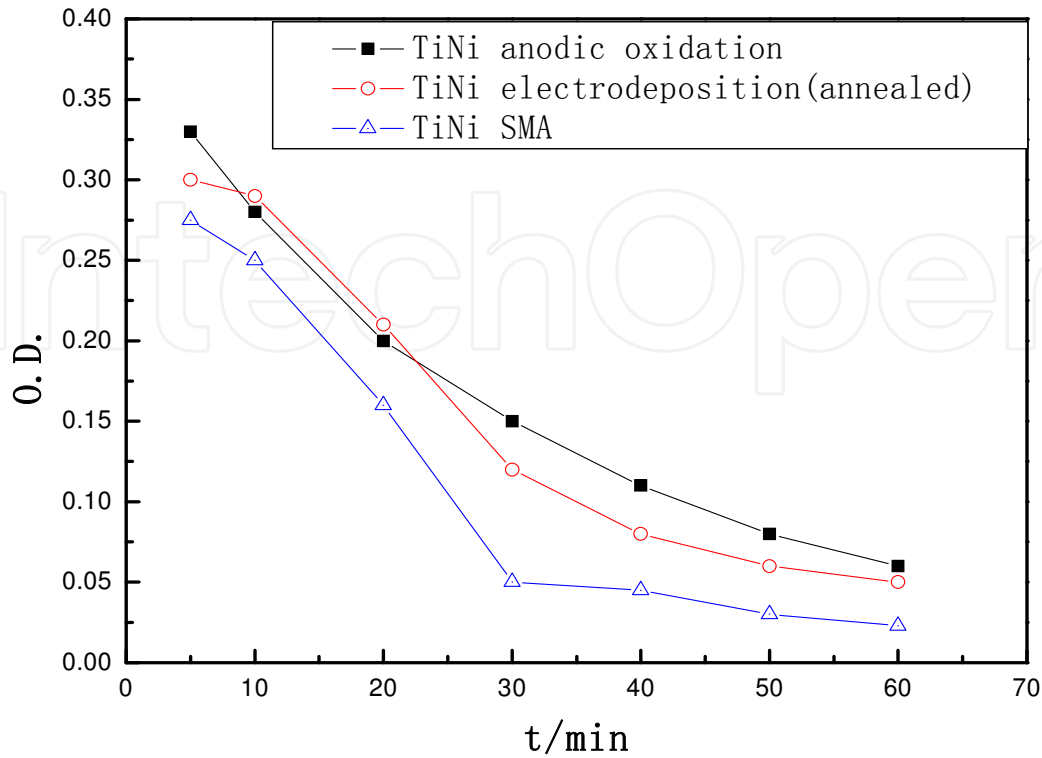


Fig. 2-5. Absorbance of modified TiNi SMA versus time

## 2.4 Summary of this chapter

1. After TiNi SMA sample anodically-oxidized was dipped in SBF solution (PH7.40) for 7d, there were more amount of Ca, P and O elements deposited on the surface. This illustrates that the capability to adsorb Ca/P layer of the anodically-oxidized sample is stronger, so TiNi SMA after anodic oxidation may have some bioactivity.
2. After TiNi SMA sample cathodically-electrodeposited was dipped in SBF solution (PH7.40) for 7d, there were higher contents of Ca and P elements deposited. The mole ratio of Ca and P reached to 2.4 : 1. And Ca and P mole ratio after crystallization at 450°C was 1.8 : 1. XRD analytical result showed that both crystallized and un-crystallized samples cathodically-electrodeposited have HA in existence. It illustrates that after the amorphous Ti-O film riching in Ti-OH group was dipped in SBF solution for 7d, HA could be formed on the surface; it also illustrates that TiO<sub>2</sub> obtained after crystallization has some bioactivity.
3. In the experiment of haemolysis rate, the haemolysis rate of surfacely-modified TiNi SMA got decreased somewhat. But the haemolysis rate of cathodically-electrodeposited sample was higher than that of anodically-oxidized one. And this was relevant to surface smoothness differences of the samples.
4. In the experiment of dynamic coagulation time, the surface modified TiNi SMA samples had a better anti-coagulation property. But the absorbance of the anodically-oxidized one was the highest, coagulation time longest, showing the best anti-coagulation property.

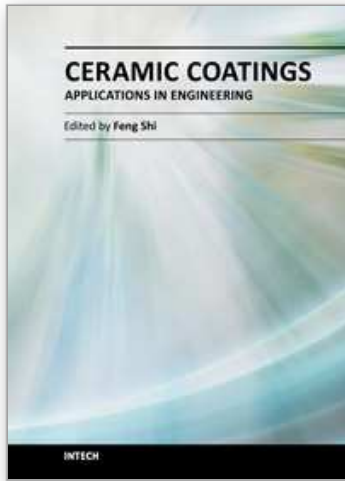
### 3. Conclusions of this paper

1. After anodic oxidization, TiNi SMA displayed a better thermodynamic stability and anti-corrosivity in simulant physiological environment, and improved blood compatibility. This laid a foundation for the biomaterial to apply in oral cavity.
2. In the self-prepared and blended well  $\text{Ti}(\text{SO}_4)_2$  electrolyte solution (PH1.2), at a constant current density of  $5\text{mA}/\text{cm}^2$ , by cathodic-electrodeposition for 4min, a layer of Ti-O film in size of dozens of nanometers had been obtained, after annealing at  $450^\circ\text{C}$ , an anatase  $\text{TiO}_2$  with bioactivity was obtained.
3. After cathodic electrodeposition, TiNi SMA displayed a better thermodynamic stability and anti-corrosivity in simulant physiological environment, and improved blood compatibility.
4. Through the discussion for Ti-O film's morphologies and properties of TiNi SMA at different technics, the optimal technical parameters obtained were: blending  $\text{Ti}(\text{SO}_4)_2$  solution to PH1-3, adding about 0.2M of  $\text{NO}_3^-$ , current density at  $5\text{mA}/\text{cm}^2$  and time for 4min.

### 4. References

- [1] Tan Xiaochun, Huang Songyu. Studies on preparation of ultrafine  $\text{TiO}_2$  membrane through electrophoretic method. Chinese journal of chemical physics[J], 1998, 11(5): 416-421
- [2] Hayward R C, Saville A, Aksay A. Electrophoretic assembly of colloidal crystals with optically tunable micropatterns[J]. Nature, 2000, 404(6733): 56-59
- [3] Kavan L, O'Regan B, Kay A, et al. Preparation of Titania (anatase) films on electrodes by anodic oxidative hydrolysis of titanium trichloride[J]. Electrical chemistry, 1993, 346(1-2):291-307
- [4] Cui Xiaoli, Jiang Zhiyu. Studies on the preparation and characteristics of titanium dioxide nano thin film. Electroplating and finishing, 2002, 21(5): 17-21
- [5] Natarajam C, Nogarni G. Cathodic electrodeposition of nanocrystalline titanium dioxide thin films[J]. J Electrochem Soc, 1996, 143(5): 1547-1550
- [6] Karuppchamy S, Amalnerkar D P, Yamaguchi K, et al. Cathodic electrodeposition of  $\text{TiO}_2$  thin films for dye-sensitized photoelectrochemical applications[J]. Materials science and engineering C, 2006, (26): 54-64
- [7] Z. D. Cui, H. C. Man, X. J. Yang. The corrosion and nickel release behavior of laser surface-melted NiTi shape memory alloy in Hanks solution[J]. Surface & coatings technology, 2005, (192): 347-353
- [8] Leung V W H, Darvell B W. Artificial salivas for in vitro studies of dental materials[J]. Journal of dentistry, 1997, 25(6): 475-484
- [9] Heng L L. Biomaterials: a forecast for the future[J]. Biomaterials, 1998, 19: 1419-1423
- [10] Xiong Xinbo, Li Hejun, Huang Jianfeng. Research progress in surface bioactivity modification of Ti-based metals[J]. Rare metals letters, 2004, 23(3): 4-9
- [11] Zhang Jingchuan. Research progress in evaluation of biomaterials' compatibility. International journal of biological engineering, 1988, 11(5): 330-334
- [12] Guo Haixia, Liang Chenghao. Research progress in materials' blood compatibility[J]. Shanghai biological engineering, 2001, 22(3): 44-48

- [13] Wang Chuanhua, Leng Xigang. Research progress in mechanism of thrombosis induced by biomaterial[J]. International journal of biological engineering, 1998, 21(1): 1-7
- [14] Liu Jingxiao. Research on preparations and structures of 316stainless and NiTi alloy surface films and their blood biocompatibilities. Doctoral thesis, Dalian university of technology, 2001
- [15] Buddy D. Ratner. Allan S. Hoffman, Frederick J. et al. Biomaterials Science: an introduction to materials in medicine, 1996, 195-197
- [16] Zhang Xiaokai, Liu Wei, Chen Xiaofeng. Mophology character of the sol-gel derived bioactive glass in SBF solution, Chinese journal of chemical physics[J], 2004, 17(4): 495-498
- [17] Liang Chenghao, Cheng Bin, Cheng Bangyi. Corrosion behavior of surface passivated Cu-Zn-Al shape memory alloy in saline solution[J]. Corrosion science and protection technology, 2005, 17(5): 304-306
- [18] Hanawa T. In vivo metallic biomaterials and surface modification[J]. Materials Science and Engineering, 1999, A (267): 260-266
- [19] Park G A. The isoelectric point of solid oxides, solid hydroxides, and aqueous hydroxy complex system[J]. Chem Rev, 1965, 65:177-198
- [20] Hench L L. Bioderamic: from concept to clinic[J]. J Am Ceram Soc, 1991, 74: 1487-1510
- [21] Kokubo T. Bioactive glass-ceramics: properties and applications[J]. biomaterials, 1991,12: 155-163
- [22] Li P, Kangasniemi I, De Groot K, et al. Bone like hydroxyapatite induction by a gel-derived titania on a titanium substrate[J]. J Am Ceram Soc, 1994, 77: 1307-1312
- [23] Fendorf M, Gronk R. Surface precipitation reaction on oxide surface[J]. J Cooloid Interface sci, 1992, 148: 295-298
- [24] Li P J, Ducheyne P. Quasi-biological apatite film induced by titanium in a simulated body fluid[J]. J Biomed Mater Res, 1998, 41: 341-148
- [25] Wang Xuejiang, Li Yubao. Study on bionic Composite of nano-HA needle-like crystals and polyamide[J]. High technology letters, 2001, 5: 1-5
- [26] Duan Yourong, Wu Yao, Wang Chaoyuan, Chen Jiyong, Zhang Xingcong. A Study of bone-like apatite formation on calcium phosphate ceramics in different kinds of animals in vivo. Journal of biomedical engineering, 2003, 20(1): 22-25
- [27] Reut godley, David starosvetsky, Irena goman. Bonelike apatite formation on niobium metal treated in aqueous NaOH[J]. Journal of materials science: Materials in medicine, 2004, 15: 1073-1077



## **Ceramic Coatings - Applications in Engineering**

Edited by Prof. Feng Shi

ISBN 978-953-51-0083-6

Hard cover, 286 pages

**Publisher** InTech

**Published online** 24, February, 2012

**Published in print edition** February, 2012

The main target of this book is to state the latest advancement in ceramic coatings technology in various industrial fields. The book includes topics related to the applications of ceramic coating covers in engineering, including fabrication route (electrophoretic deposition and physical deposition) and applications in turbine parts, internal combustion engine, pigment, foundry, etc.

### **How to reference**

In order to correctly reference this scholarly work, feel free to copy and paste the following:

Zhu Weidong (2012). Ti-O Film Cathodically-Electrodeposited on the Surface of TiNi SMA and Its Bioactivity and Blood Compatibility, Ceramic Coatings - Applications in Engineering, Prof. Feng Shi (Ed.), ISBN: 978-953-51-0083-6, InTech, Available from: <http://www.intechopen.com/books/ceramic-coatings-applications-in-engineering/ti-o-film-cathodically-electrodeposited-on-the-surface-of-tini-sma-and-its-bioactivity-and-blood-com>

**INTECH**  
open science | open minds

### **InTech Europe**

University Campus STeP Ri  
Slavka Krautzeka 83/A  
51000 Rijeka, Croatia  
Phone: +385 (51) 770 447  
Fax: +385 (51) 686 166  
[www.intechopen.com](http://www.intechopen.com)

### **InTech China**

Unit 405, Office Block, Hotel Equatorial Shanghai  
No.65, Yan An Road (West), Shanghai, 200040, China  
中国上海市延安西路65号上海国际贵都大饭店办公楼405单元  
Phone: +86-21-62489820  
Fax: +86-21-62489821

© 2012 The Author(s). Licensee IntechOpen. This is an open access article distributed under the terms of the [Creative Commons Attribution 3.0 License](#), which permits unrestricted use, distribution, and reproduction in any medium, provided the original work is properly cited.

IntechOpen

IntechOpen